

The P4-ATPase Drs2 interacts with and stabilizes the multisubunit tethering complex TRAPPIII in yeast

Irene Pazos¹ , Marta Puig-Tintó¹, Laura Betancur¹, Jorge Cordero¹ , Nereida Jiménez-Menéndez¹, Marc Abella¹, Altair C Hernández¹, Ana G Duran¹, Emi Adachi-Fernández¹, Carla Belmonte-Mateos¹, Susana Sabido-Bozo^{2,3} , Sébastien Tosi⁴, Akiko Nezu^{5,6} , Baldomero Oliva^{1,7}, Julien Colombelli⁴, Todd R Graham⁸, Tamotsu Yoshimori^{5,6} , Manuel Muñiz^{2,3} , Maho Hamasaki^{5,6} & Oriol Gallego^{1,*} 

Abstract

Multisubunit Tethering Complexes (MTCs) are a set of conserved protein complexes that tether vesicles at the acceptor membrane. Interactions with other components of the trafficking machinery regulate MTCs through mechanisms that are partially understood. Here, we systematically investigate the interactome that regulates MTCs. We report that P4-ATPases, a family of lipid flippases, interact with MTCs that participate in the anterograde and retrograde transport at the Golgi, such as TRAPPIII. We use the P4-ATPase Drs2 as a paradigm to investigate the mechanism and biological relevance of this interplay during transport of Atg9 vesicles. Binding of Trs85, the sole-specific subunit of TRAPPIII, to the N-terminal tail of Drs2 stabilizes TRAPPIII on membranes loaded with Atg9 and is required for Atg9 delivery during selective autophagy, a role that is independent of P4-ATPase canonical functions. This mechanism requires a conserved I(S/R)TTK motif that also mediates the interaction of the P4-ATPases Dnf1 and Dnf2 with MTCs, suggesting a broader role of P4-ATPases in MTC regulation.

Keywords Atg9; Cvt pathway; Drs2; TRAPPIII; vesicle transport

Subject Categories Autophagy & Cell Death; Membrane & Trafficking

DOI 10.15252/embr.202256134 | Received 16 September 2022 | Revised 10 February 2023 | Accepted 17 February 2023

EMBO Reports (2023) e56134

Introduction

Multisubunit tethering complexes (MTCs) are a group of protein complexes essential for vesicle transport. Multisubunit tethering complexes mediate the tethering of the vesicle to the acceptor membrane through long-range interactions that precede vesicle fusion and cargo delivery at the destination of the transport pathway (Yu & Hughson, 2010; Bröcker *et al.*, 2010). Eight MTCs have been described in yeast, all conserved in humans (Dubuke & Munson, 2016). The conserved oligomeric Golgi (COG) complex is involved in intra-Golgi retrograde transport (Suvorova *et al.*, 2002). Dsl1 is responsible for tethering COPI vesicles derived from the Golgi to the endoplasmic reticulum (ER) (Ren *et al.*, 2009). The class C core vacuole/endosome tethering (CORVET) complex and the homotypic fusion and vacuole protein sorting (HOPS) complex act at the endosomal/vacuolar pathway where CORVET tethers vesicles at early endosomes and HOPS functions in late endosomes and the vacuole (Balderhaar & Ungermann, 2013). The Golgi-associated retrograde protein (GARP) complex tethers vesicles derived from endosomes to the trans-Golgi network (TGN) (Conibear *et al.*, 2002). The exocyst is responsible for tethering secretory vesicles to the plasma membrane (Heider *et al.*, 2016). Finally, the transport protein particle (TRAPP) complexes have historically been classified as MTCs despite their major role as guanine nucleotide exchange factors for Rab GTPases (Yu & Liang, 2012). The transport protein particle comes in two flavors: TRAPP II and TRAPP III (Thomas *et al.*, 2018). Both complexes have a heterohexameric core called TRAPPI. TRAPP II, with four more specific subunits (Yip *et al.*, 2010), activates Ypt31/32 to regulate intra-Golgi transport (Morozova *et al.*, 2006). TRAPP III, with the sole-specific subunit Trs85 (Tan *et al.*, 2013), activates Ypt1 to

¹ Department of Medicine and Life Sciences (MELIS), Pompeu Fabra University (UPF), Barcelona, Spain

² Department of Cell Biology, University of Seville, Seville, Spain

³ Instituto de Biomedicina de Sevilla (IBiS), Hospital Universitario Virgen del Rocío/CSIC/Universidad de Sevilla, Seville, Spain

⁴ Institute for Research in Biomedicine (IRB Barcelona), The Barcelona Institute of Science and Technology (BIST), Barcelona, Spain

⁵ Department of Genetics, Graduate School of Medicine, Osaka University, Osaka, Japan

⁶ Department of Intracellular Membrane Dynamics, Graduate School of Frontier Biosciences, Osaka University, Osaka, Japan

⁷ Structural Bioinformatics Lab (GRIB-IMIM), Barcelona, Spain

⁸ Department of Biological Sciences, Vanderbilt University, Nashville, TN, USA

*Corresponding author. Tel: +34 933160849; E-mail: oriol.gallego@upf.edu

regulate the transport of ER-derived COPII vesicles to the Golgi (Tan *et al*, 2013). The function of MTCs requires the interaction with other components of the trafficking machinery such as GTPases, SNAREs, and Sec1/Munc18 (SM) proteins (Bröcker *et al*, 2010; Yu & Hughson, 2010). However, studies have been centered on the mechanism of individual MTCs, which limited the understanding of the molecular bases that play a general role in MTCs function.

To shed light on the molecular mechanisms that regulate MTCs, we have systematically searched for interactions that are functionally relevant for these protein complexes in yeast. Our approach combines genetic interactions and PICT (Protein interactions from Imaging Complexes after Translocation), a live-cell imaging method that can detect low abundant interactions (Gallego *et al*, 2013; Torreira *et al*, 2017). We found that MTCs involved in the anterograde and retrograde transport at the Golgi (COG, GARP, TRAPP1, and TRAPP3) bind Type IV P-type ATPases (P4-ATPases), a family of lipid flippases that maintain membrane lipid asymmetry by translocating and accumulating phospholipids to the cytosolic leaflet.

COG, GARP, TRAPP1, and TRAPP3 are involved in the transport of the Autophagy-related protein 9 (Atg9) (Reggiori *et al*, 2003; Shirahama-Noda *et al*, 2013; Zou *et al*, 2013; Wang *et al*, 2017), a transmembrane lipid scramblase (Matoba *et al*, 2020; Sawamakarska *et al*, 2020) essential for the Cytoplasm-to-vacuole targeting (Cvt) pathway. The Cvt pathway is used as a model to study selective autophagy, a set of pathways that target the degradation of cellular components in a specific manner to maintain the cell fitness. The Cvt pathway initiates with the construction of the PAS (pre-autophagosomal structure). Then, a double membrane elongates from the PAS to envelop the precursor Ape1 (prApe1) aminopeptidase until the double membrane closes generating the Cvt vesicle. After fusion and internalization in the vacuole, the prApe1 is cleaved to mature Ape1 (mApe1) (Lynch-Day & Klionsky, 2010; Guimaraes *et al*, 2015). In growing cells, Atg9 cycles in cytoplasmic vesicles between Atg9 reservoirs at the endocytic compartments and the Golgi (Yamamoto *et al*, 2012). However, when the Cvt pathway is triggered, Atg9 is transported to the PAS, a step that is strictly required for the *de novo* formation of the Cvt vesicle (Shirahama-Noda *et al*, 2013).

Among the MTCs involved in the transport of Atg9, the function of TRAPP3 is essential for the Cvt pathway. TRAPP3 is responsible for Atg9 vesicular transport from early endosomes to the Golgi, allowing Atg9 transport to the PAS (Shirahama-Noda *et al*, 2013). Thus, in *trs85Δ* cells, Atg9 does not reach the PAS, the biogenesis of the Cvt vesicle is blocked and the prApe1 accumulates in large cytosolic aggregates (Meiling-Wesse *et al*, 2005; Shirahama-Noda *et al*, 2013). The mechanisms regulating the function of TRAPP3 during the transport of Atg9 vesicles from the reservoirs remain elusive (Yamamoto *et al*, 2012).

We challenged the functional relevance of the interactions between MTCs and P4-ATPases by studying the role of the TRAPP3-Drs2 assembly in the transport of Atg9. Drs2 is a P4-ATPase located at the TGN and early endosomes that flips phosphatidylserine (PS) specifically (Natarajan *et al*, 2004; Hanamatsu *et al*, 2014). Here, we show that Drs2 regulates TRAPP3 in the transport of Atg9, a role that is independent of Drs2 reported functions. Cross-linking and competitive assays demonstrate that proximal binding to the N-terminal tail of Drs2 stabilizes TRAPP3 on membranes loaded with Atg9, which is necessary for the transport of Atg9 for

the early stages of the Cvt pathway. We demonstrate that Drs2 is required for the biogenesis of Atg9 vesicles from the reservoirs through a mechanism that requires the I(S/R)TTK motif located in its N-terminal tail. This motif is conserved in other flippases and is crucial to sustain the network of interactions between P4-ATPases and MTCs.

Results

Protein–protein interactions relevant for MTCs function

In an effort to thoroughly explore the space of protein interactions that are relevant for MTCs function, we conducted a genome-wide search based on reported genetic interactions in yeast (Costanzo *et al*, 2011; Data ref: Saccharomyces Genome Database, 2013). Genes coding for MTCs subunits establish 2,587 genetic interactions with 1,283 other genes. Based on the probability of these genetic interactions to occur randomly, we selected those gene products that are more likely to be functionally linked with MTCs and that have not been shown to bind MTCs before. Overall, we selected 426 proteins for subsequent protein–protein interaction screening (Dataset EV1, see Materials and Methods).

We then used the PICT assay to screen interactions directly in living cells (Gallego *et al*, 2013; Torreira *et al*, 2017; Fig 1A). PICT is based on the rapamycin-induced heterodimerization of the FK506-binding protein (FKBP) and the FKBP-rapamycin binding (FRB) domain (Chen *et al*, 1995; Gallego *et al*, 2013). The addition of rapamycin to the media induces the translocation of proteins tagged with FRB (bait-FRB) to intracellular anchoring platforms tagged with FKBP and RFP (anchor-RFP-FKBP). In our strains rapamycin has no effect on endogenous TORC1 as this has been mutated to the rapamycin-insensitive form *tor1-1* (see Materials and Methods). If a GFP-tagged protein (prey-GFP) interacts with the bait-FRB, it will build-up at the anchor upon addition of rapamycin, which can be quantified by the increment in the co-localization of the GFP and RFP signals. In a previous study, we enhanced PICT sensitivity up to 200-fold by engineering yeast cells to express anchoring platforms at the spindle pole body (Tub4-RFP-FKBP). By tagging Tub4 with RFP and FKBP, the resulting cells harbor one or two anchoring platforms only. Thus, even low abundant complexes accumulate enough prey-GFP in the anchoring platforms to be efficiently detected and quantified (Torreira *et al*, 2017). The PICT assay cannot discern between direct and indirect interactions. However, among the 426 proteins screened, there is extensive redundancy of the subcellular localization. The selective binding patterns detected minimize the possibility that the PICT assay generally reports unspecific interactions resulting from the anchoring of entire membrane compartments.

The screen identified seven proteins, all conserved in humans, which establish eight protein–protein interactions with MTCs (Fig 1B and C). The COG complex binds Snc2, an exocytic SNARE known to traffic through the Golgi (Protopopov *et al*, 1993). CORVET binds Hse1, Bro1, Vps45, and Vps9, all involved in the sorting of vacuolar proteins. These interactions provide molecular bases to the mechanism that underlies the interplay between CORVET and the Vps9-Vps21-Vps45 module (Balderhaar *et al*, 2013; Zhou *et al*, 2017). We also found that TRAPP1 and TRAPP3 bind

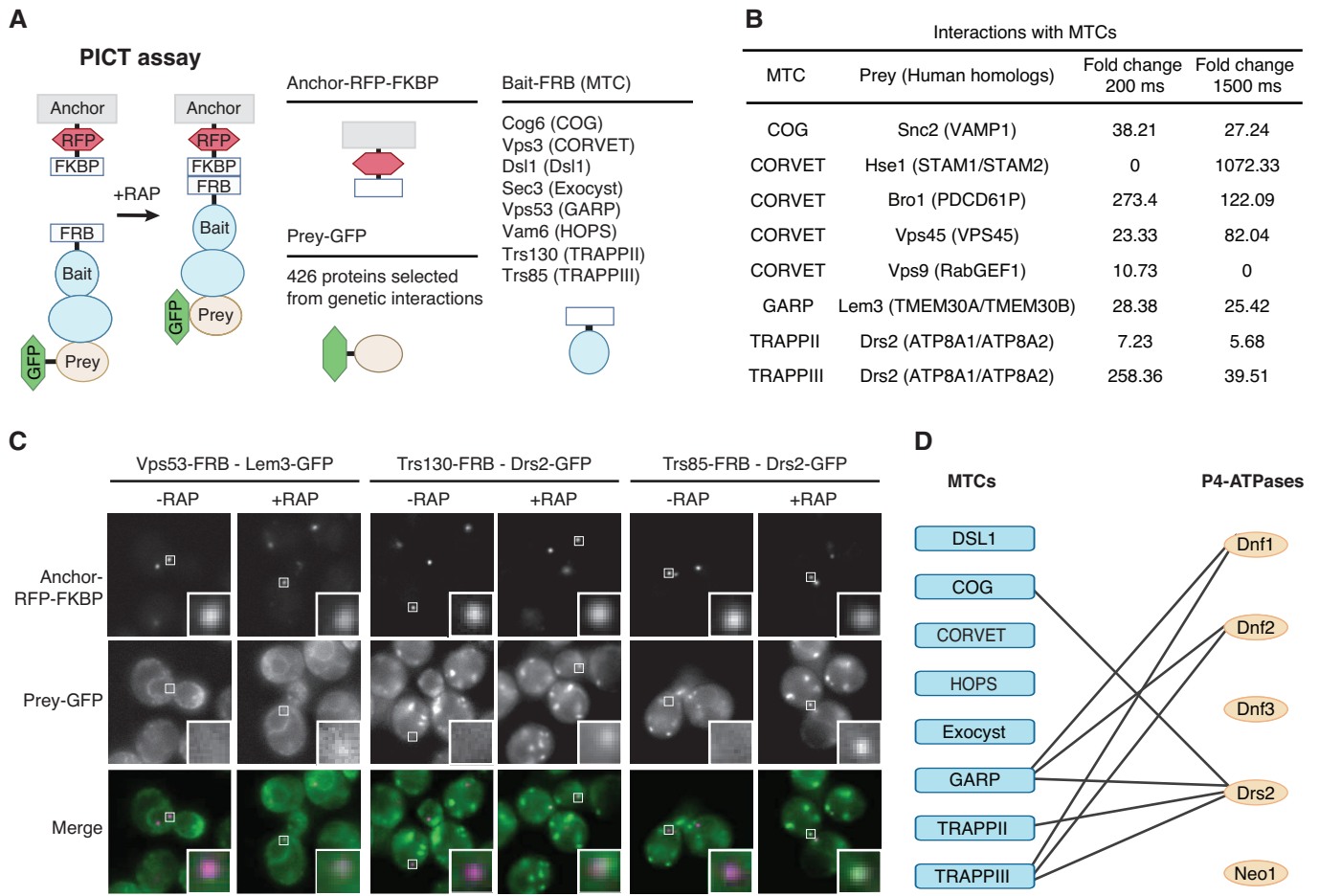


Figure 1. PICT assay and protein–protein interactions relevant for MTCs function.

- A Illustration of the PICT assay (left). Most efficient baits used to anchor each MTC (in parenthesis) are listed (top right) (see Dataset EV2).
- B Summary of detected protein–protein interactions and Fold change obtained (see Dataset EV1). Human homologs are indicated in parenthesis.
- C PICT assay for the interactions between indicated pairs of proteins tagged to FRB and GFP. Representative images before and after adding rapamycin (RAP) of RFP-tagged anchor and GFP-tagged prey are shown in the upper and middle row, respectively. Bottom row shows the merged images. White zoom in boxes, 0.9 μ m. Scale bar, 5 μ m.
- D Network of interactions between MTCs and P4-ATPases. MTCs are represented by blue boxes and P4-ATPases by orange oval circles. Black lines show the interactions found with PICT.

Drs2, while GARP interacts with Lem3. Drs2 is one of the five yeast P4-ATPases together with Dnf1, Dnf2, Dnf3, and Neo1. Except for the last one, all P4-ATPases act as heterodimers with its β -subunit: Lem3 for Dnf1 and Dnf2; Cdc50 for Drs2; and Crf1 for Dnf3 (Saito *et al.*, 2004; Sebastian *et al.*, 2012). Thus, the screen identified three MTCs that could bind to P4-ATPases, suggesting a general mechanism underlying these interactions (Dataset EV1 and Fig 1B and C).

The network of interactions between MTCs and P4-ATPases

To gain a more comprehensive view of the relationship between MTCs and P4-ATPases, we expanded the study of interactions to all MTCs and P4-ATPases (Fig 1D). Detected binding events define a network with specific configuration of interactions. GARP and TRAPPIII concentrate most of the interactions with the P4-ATPases

Drs2, Dnf1, and Dnf2, flippases that circulate between the plasma membrane and the Golgi. These interactions provide a molecular basis for the recycling of Dnf1 and Dnf2 mediated by GARP (Eising *et al.*, 2019). Note that Dnf1 and Dnf2, known to have redundant functions (Hua *et al.*, 2002), also show identical binding specificity with MTCs. In addition to GARP, TRAPPII, and TRAPPIII, Drs2 also interacts with COG, being the flippase that shows the highest number of interactions with MTCs.

Overall, MTCs involved in trafficking pathways at the Golgi show preference to bind Drs2, Dnf1, and Dnf2, whereas we could not detect binding with other proteins found at this organelle (i.e., Sec7 and Vps10, Fig EV1). These results raise the possibility that binding to P4-ATPases might be involved in the molecular mechanisms that COG, GARP, TRAPPII, and TRAPPIII use to control vesicle transport in the Golgi. To better understand the molecular mechanism that

regulates MTCs function, we further investigated the interactions with Drs2, the only P4-ATPase whose atomic structure was available at the time of this study (Bai *et al*, 2019; Timcenko *et al*, 2019a).

Drs2 regulates the biogenesis of the Cvt vesicle

We investigated the functional relationship between TRAPPIII and Drs2. In cells lacking TRAPPIII subunit Trs85 (*trs85Δ*), Atg9 is not delivered to the PAS, the biogenesis of the Cvt vesicle is blocked, and Ape1 is accumulated in large cytosolic aggregates (Meiling-Wesse *et al*, 2005; Shirahama-Noda *et al*, 2013; Fig 2A and B). The cellular relevance of Drs2 varies at different growing temperatures: Drs2 is essential for cell growth below 21°C (although cells remain viable) (Chen *et al*, 1999), whereas the flippase is dispensable at higher temperatures. Therefore, we first analyzed the contribution of Drs2 in the Cvt pathway at different temperatures. While Ape1 processing is fully blocked in *trs85Δ* cells incubated at any of the temperatures tested, cells lacking Drs2 (*drs2Δ*) show a progressive inhibition of Ape1 maturation when decreasing the temperature. Thus, *drs2Δ* cells process Ape1 near to normality at 37°C, while we could only detect traces of mApe1 in cells incubated at 16°C (Fig 2A and EV2A and B). Accordingly with a specific role of Drs2 at low temperatures, the processing of Ape1 in wild-type cells at 16°C was normal (Fig EV2B). We continued studying the interplay between Drs2 and TRAPPIII at 23°C to avoid undesired effects derived from impaired cell fitness. At this temperature, *drs2Δ* cells mature 12% of the aminopeptidase (Fig 2A). We confirmed that such levels of mApe1 represent the steady-state levels of the Cvt pathway in mutant cells incubated at 23°C by analyzing Ape1 processing in cells lacking Drs2 and Atg19 (i.e., specific receptor for the Cvt pathway), Drs2 and Atg17 (i.e., specific scaffold for nonselective autophagy) and in a time course assay (Fig EV2C and D). Consistently with a functional relationship between TRAPPIII and Drs2, cells lacking either Trs85 or Drs2 accumulate similar Ape1-GFP aggregates (Fig 2B).

PICT assay showed that, concomitantly to an exacerbation of the Drs2 role in the Cvt pathway, the Drs2-TRAPPIII interaction is boosted under colder conditions: at 23°C the Interaction score between Drs2 and Trs85 is 24% higher than at 37°C (Fig 2C), while no significant difference could be detected for the interaction between Trs85 and Bet5, a subunit of TRAPPI core. This observation suggests that the cell regulates the interplay between Drs2 and TRAPPIII in response to temperature shifts.

We then used electron microscopy (EM) to study the ultrastructure of the Cvt pathway in the absence of Drs2. To figure out whether defects in Ape1 processing result from a defective vacuolar function, we mutated Pep4. Pep4 is a protease required for the processing of the Cvt vesicle once it is internalized in the vacuole (Baba *et al*, 1997). While 89.3% of the *pep4Δ* cells presented Cvt bodies inside the vacuole, we could not detect any Cvt body-like structure in the vacuoles of *pep4Δdrs2Δ* cells (Fig 2D), indicating that Ape1 processing defect originates before the Cvt cargo is delivered to the vacuole.

We then analyzed Ape1-GFP aggregates in *drs2Δ* cells with Correlative Light and Electron Microscopy (CLEM) (Kukulski *et al*, 2011). 94.8% of the Ape1-GFP spots that were analyzed correlated with a ribosome exclusion area of amorphous shape and that was

devoid of double membrane or Cvt vesicle-like structure (Fig 2E). In agreement, we could not detect Ape1-GFP aggregates in the vacuole of *drs2Δ* cells stained with FM4-64 and imaged by fluorescent microscopy (Movie EV1). Overall, these results demonstrate that Drs2 is necessary for the early stages of the biogenesis of the Cvt vesicle, a role that is further underscored by the enrichment of DRS2 genetic interactions with genes coding for proteins involved in autophagy (51 genes of 571, $P = 7 \times 10^{-5}$).

The role of Drs2 in the Cvt pathway is independent from known mechanisms

Drs2 is a lipid flippase with multiple functions in vesicle transport at the interface of endosomes and the Golgi (Natarajan *et al*, 2004; Hanamatsu *et al*, 2014). We used yeast genetics to investigate the possibility that defects in the Cvt pathway in *drs2Δ* cells result indirectly from the perturbation of other processes regulated by the flippase. However, Ape1 processing was not hindered in cells lacking Rcy1 (i.e., cells where the transport from early endosomes to TGN is blocked; Furuta *et al*, 2007; Hanamatsu *et al*, 2014), Apl4 (i.e., cells where the AP-1 pathway from TGN to early endosomes and the exit of the high-density class of vesicles from the TGN are blocked; Hinners, 2003; Liu *et al*, 2008), Apl5 (i.e., cells where ALP pathway from TGN to the vacuole is blocked; Odorizzi *et al*, 1998) or both Gga1 and Gga2 (i.e., cells where CPY pathway from TGN to late endosomes is blocked; Sakane *et al*, 2006; Fig 3A). Thus, genetic data suggest that the biogenesis of the Cvt vesicle does not involve the pathways where Drs2 has been reported to participate.

We then explored the molecular mechanism of Drs2 that is required for the biogenesis of the Cvt vesicle. We analyzed the Ape1 processing in *drs2Δ* cells expressing different constructs of Drs2 (Fig 3B). All the constructs employed in this study to express Drs2 used the control of DRS2 promoter. We first targeted the PS flipping activity of Drs2, which is required for the bidirectional transport endosome-TGN and for the exit of secretory vesicles from the TGN (Alder-Baerens *et al*, 2006; Liu *et al*, 2008; Xu *et al*, 2013). While cells harboring an empty vector do not improve Ape1 processing in *drs2Δ* cells, cells expressing a mutant unable to flip PS (*drs2-GA*) and cells expressing an ATPase-dead mutant of Drs2 (*drs2-D560N*) rescue either totally or partially the Cvt pathway (Fig 3C). Cells lacking Cho1, an enzyme essential for the synthesis of PS (Choi *et al*, 2010), show normal processing of Ape1, confirming that flipping of PS is not required for the Cvt pathway (Fig 3D).

The cytosolic C-terminal tail of the flippase is also important for the known functions of Drs2. For instance, the Gea2 interacting motif (GIM) formed by the LSSLVMK sequence (Chantalat, 2004), is required for the Drs2-Gea2-Arl1 complex assembly, a mechanism based on protein-protein interactions that regulate a number of trafficking pathways at the TGN and endosomes (Chantalat, 2004; Tsai *et al*, 2013). Adjacent to the GIM, Drs2 presents a conserved motif (CM). Conserved motif is fundamental for Drs2 function and to bind to the cytosolic domains of Drs2 that stabilize the autoinhibitory conformation (Chantalat, 2004; Timcenko *et al*, 2019a). Drs2 has also two NPFXD motifs (hereafter referred to as NPF motif) that constitute some of its multiple endocytosis signals (Liu *et al*, 2007). However, expression of *drs2-ΔGIM*, *drs2-ΔCM* or *drs2-ΔGIMΔNPF* also show more than 50% of Ape1 processing (Fig 3E). Thus, the mutagenesis experiments indicate that known functional motifs of

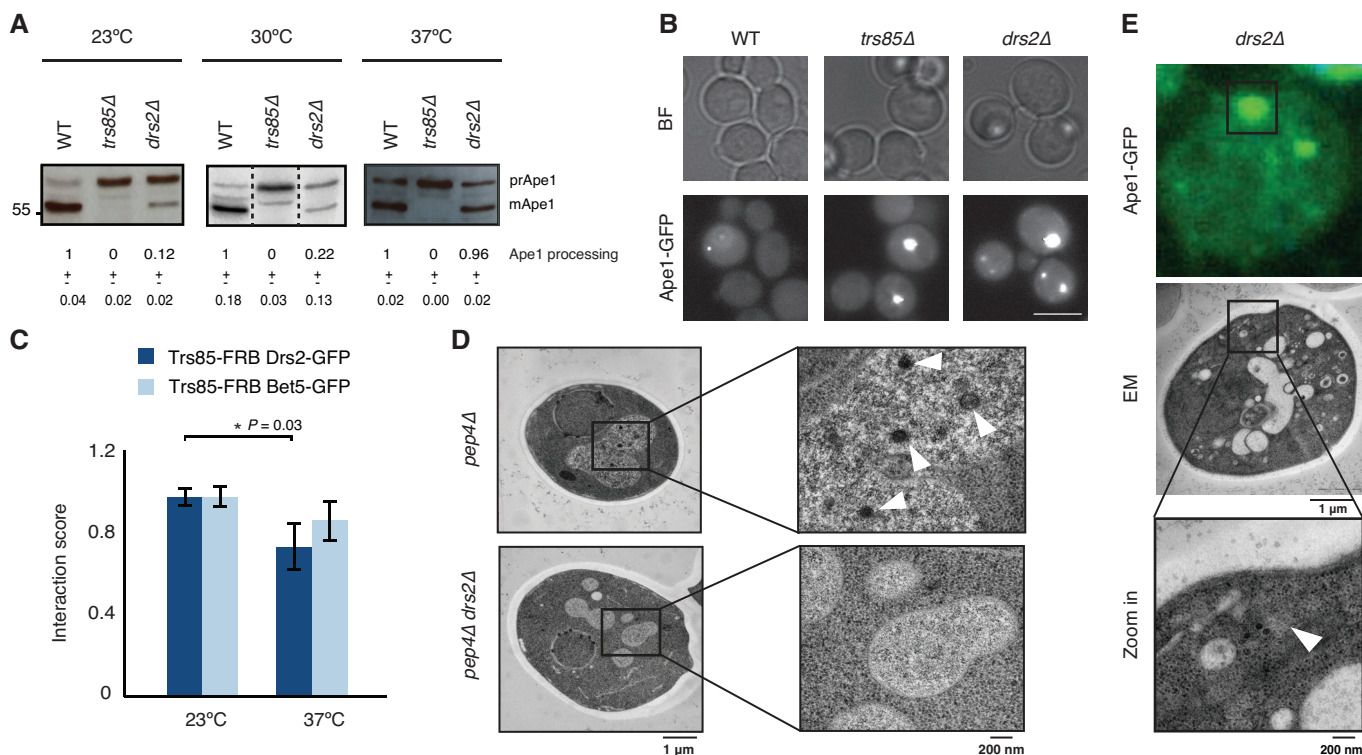


Figure 2. Drs2 is critical for the biogenesis of the Cvt vesicle.

A Ape1 processing was analyzed by Western blot in the indicated strains and temperatures and normalized to the processing achieved in wild-type cells \pm SD, $n = 3$.
 B Aggregation of Ape1. Representative images of Ape1-GFP in wild-type, *trs85Δ* and *drs2Δ* cells. BF, brightfield images. Scale bar, 5 μ m.
 C PICT assay for the interaction of Trs85-FRB with Drs2-GFP or Bet5-GFP. The interaction score was normalized to the measurement at 23°C. Error bars: mean \pm SD, $n = 3$. Asterisk indicates significant difference as determined by a two-tailed Student's *t*-test ($P < 0.05$).
 D Representative EM images of *pep4Δ* and *pep4Δ drs2Δ* strains. Black squares show a zoom-in in the vacuole. White arrowheads point to Cvt bodies.
 E Representative CLEM images of *drs2Δ* cells. Ape1-GFP (top) correlates with a membrane-free ribosome exclusion area (middle). Black square (bottom) shows a zoom-in at the position correlating with Ape1-GFP (white arrowhead).

Data information: $n =$ biological replicate.

the Drs2 C-terminal tail are not essential for the role of the flippase in the Cvt pathway.

The I(S/R)TTK motif is required for the function of Drs2 in the Cvt pathway

We then investigated the cytosolic N-terminal tail of Drs2. Although P4-ATPases present low homology in this region, multiple sequence alignment identified a conserved stretch of 15 amino acids (residues 198–212 in Drs2; Fig 4A). The stretch defines a cavity of 18.8 Å in depth located adjacent to the first transmembrane helix in the structure of Drs2 (Fig 4B). Homology modeling suggests that all yeast P4-ATPases present the N-terminal cavity in their structure (Fig EV3), although the function of this cavity is not known. We observed that the bottom of the cavity of those P4-ATPases that bind MTCs (Dnf1, Dnf2, and Drs2) is characterized by an I(S/R)TTK motif that is lacking in the cavity of Dnf3 and Neo1 (Fig 4A). The correlation between this structural feature and the P4-ATPases-MTCs interaction pattern suggested that the I(S/R)TTK motif might be relevant for the function of P4-ATPases as regulatory partners of MTCs.

We first generated cells expressing Drs2 with its I(S/R)TTK motif substituted by five alanines (*drs2-5A*). The expression of *drs2-5A*

rescues the cold-sensitive phenotype of *drs2Δ* cells, confirming that the loss of this motif does not induce general protein unfolding (Fig 4C). In agreement, comparative co-localization of Drs2-GFP and *drs2-5A*-GFP with Sec7-RFP, a marker of the TGN, shows that *drs2-5A*-GFP is properly transported to the Golgi (Fig EV4A). However, the expression of *drs2-5A* in *drs2Δ* cells cannot rescue Ape1 processing (Fig 4D), which accumulates in large cytosolic Ape1-GFP aggregates similar to those seen in *trs85Δ* and *drs2Δ* cells (Movie EV2). These results prompted us to investigate the molecular bases that control the function of the Drs2 I(S/R)TTK motif.

Drs2 I(S/R)TTK mediates proximal interactions with MTCs

We first designed a competition assay to corroborate that Drs2 function in the Cvt pathway is mediated by interactions with its N-terminal tail. We measured the impact on Ape1 processing of overexpressing amino acids 1–212 of Drs2, which include the I(S/R)TTK motif. Remarkably, overexpression of Drs2 N-terminal tail caused a 30% inhibition of Ape1 processing (Fig 5A).

Then, to systematically analyze the mechanism mediated by the Drs2 I(S/R)TTK motif, we carried out cross-linking-mass spectrometry (XL-MS) immunoprecipitation experiments (see Materials and

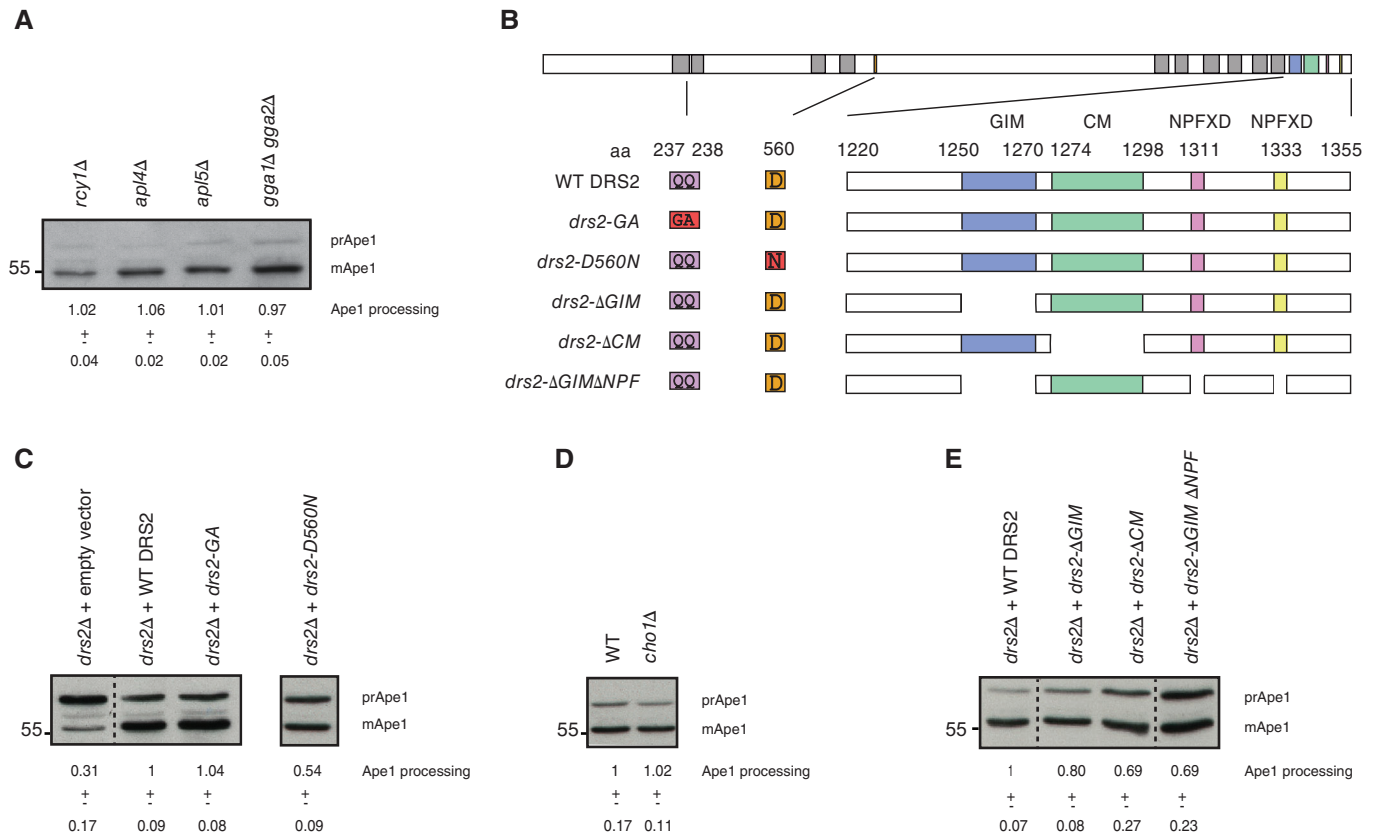


Figure 3. Drs2 role in the Cvt pathway is independent from its known mechanisms.

A–E (A, C, E) Ape1 processing was analyzed by Western blot in the indicated strains, and normalized to the processing achieved in cells expressing wild-type Drs2 \pm SD, $n \geq 3$ biological replicates. (B) Representation of the main structural features of Drs2. Each color in the top bar indicates the location of the features in the sequence of wild-type Drs2. Gray boxes depict transmembrane domains. Below, a summary of the mutants tested and an enlarged view of their C-terminal tail. QQ > GA and D > N mutations are depicted in red. Numbers indicate the residues position in Drs2 sequence. (D) Ape1 processing was analyzed by Western blot in the indicated strains, and normalized to the processing achieved in wild-type cells \pm SD, $n = 3$ biological replicates.

Methods). We performed a partial cross-linking with disuccinimidyl sulfoxide (DSSO), a cross-linker of 10.1 Å in length that allowed us to detect proximal peptides in cell extracts (Kao *et al*, 2011). Upon a GFP-specific pulldown, the comparative analysis between the interactome of Drs2-GFP and *drs2-5A*-GFP identified 26 proteins that are likely to recognize directly, or in the near vicinity, Drs2-GFP and whose binding requires the I(S/R)TTK motif (Fig EV4B). This set of interactions is enriched with proteins involved in endosomal transport ($P = 3.9 \text{ E-}06$), Golgi vesicle transport ($P = 3.5 \text{ E-}05$), and endosome-to-Golgi transport ($P = 4.9 \text{ E-}08$). In agreement with the cold-sensitivity rescue assay (Fig 4C), known protein–protein interactions required for canonical Drs2 functions were not affected by Drs2 mutation (e.g., binding to Cdc50 or Rcy1). Overall, our results suggest that the mutation of the I(S/R)TTK motif allows us to dissect different mechanisms controlled by Drs2.

Although Drs2-GFP pulled down subunits of the GARP, TRAPPII, and TRAPPIII complexes, we could not detect binding of Drs2-GFP to any subunit of the COG complex in the XL-MS experiments, suggesting that Drs2 and COG do not interact directly. Interestingly, *drs2-5A*-GFP could not recapitulate the interaction with Trs85 (the specific subunit of TRAPPIII), and the interactions with Trs65,

Trs120, Trs130 (specific subunits of TRAPPII) and Vps53 (GARP) were also destabilized upon mutation of the I(S/R)TTK motif. Thus, the interactome data suggest that the I(S/R)TTK motif plays a role in the network of interactions between Drs2 and GARP, TRAPPII, and TRAPPIII (Figs 5B and EV4B). We further confirmed this observation using PICT. Although our assay was not sensitive enough to recapitulate the interaction between Drs2-GFP and GARP in Δ *drs2* cells expressing Drs2 from a centromeric plasmid, PICT confirmed that the lack of the I(S/R)TTK motif abrogated the interaction between the lipid flippases and TRAPPII and TRAPPIII (Fig 5C and EV4C). These results encouraged us to investigate the general contribution that the I(S/R)TTK motif might have in the network of interactions between P4-ATPases and MTCs.

A general mechanism for the interplay between P4-ATPases and MTCs

The N-terminal tail of P4-ATPases is composed of a large unstructured region that is not conserved and a stretch of 15 amino acids that define the cavity that links the first transmembrane helix and the unstructured region (Timcenko *et al*, 2019a). We cannot exclude

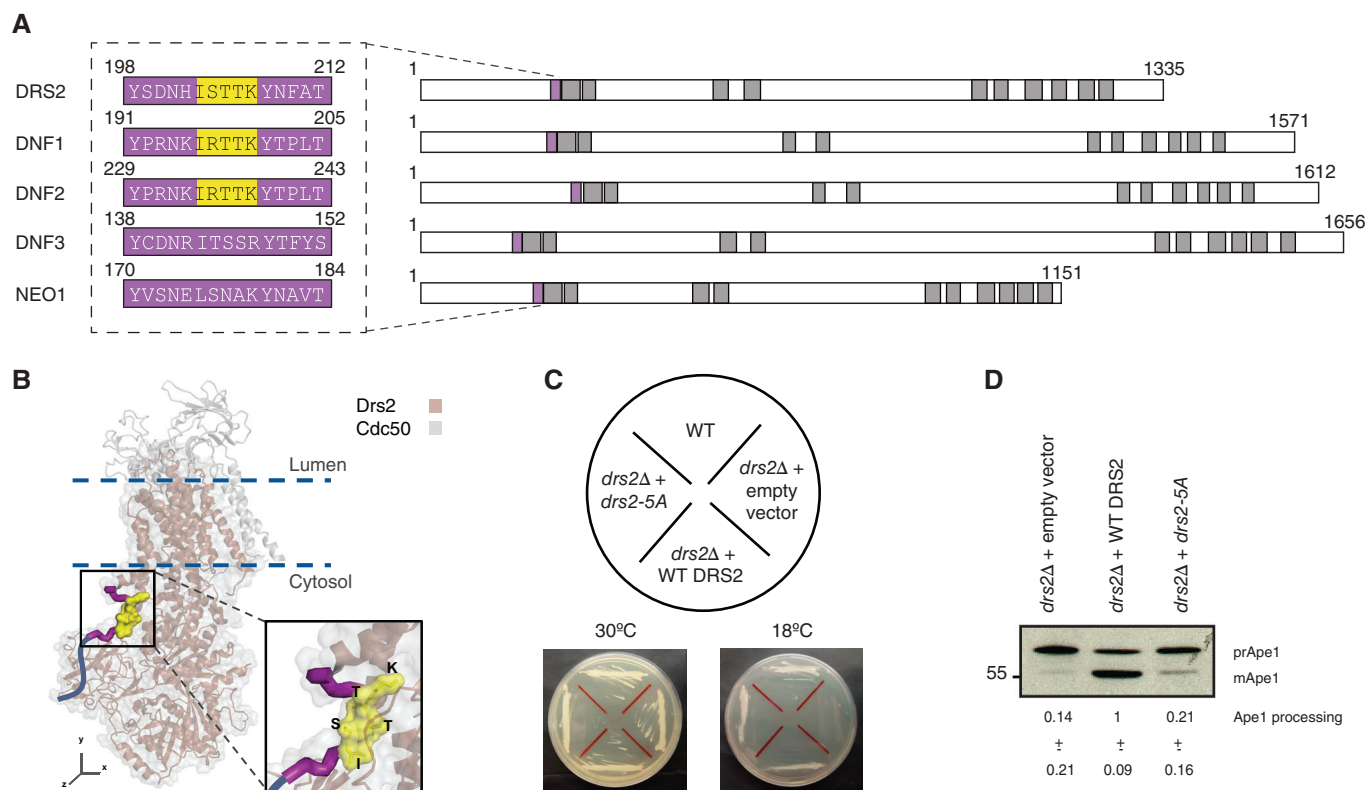


Figure 4. The I(S/R)TTK motif is required for the interaction between Drs2 and TRAPPIII and its function in the Cvt pathway.

A Representation of the 15 amino acid (aa) cavity (purple) in the N-terminal tail of P4-ATPases. Gray boxes depict transmembrane domains. Black dashed box shows the sequence coding for the cavity (left). Yellow background highlights the I(S/R)TTK motif in Drs2, Dnf1 and Dnf2.

B The I(S/R)TTK motif in the Drs2-Cdc50 structure (PDB ID: 6ROH; Timcenko *et al.*, 2019a; Data ref: Timcenko *et al.*, 2019b). Black box zooms in the cavity of Drs2 (purple) and the I(S/R)TTK motif (yellow). Dark blue line depicts the unstructured N-terminal region.

C Cold-sensitive assay for the indicated strains. Cells streaked onto YPD plates were incubated at 30 and 18°C for 3 days.

D Ape1 processing was analyzed by Western blot in the indicated strains, and normalized to the processing achieved in cells expressing wild-type Drs2 \pm SD, $n = 3$ biological replicates.

that MTCs bind the unstructured region of the P4-ATPases N-terminal tail. However, the lack of sequence homology among the P4-ATPases that bind MTCs hints that this is unlikely to be a universal mechanism. Alternatively, MTCs might bind the N-terminal cavity of P4-ATPases that nest the I(S/R)TTK motif. Although it has no known function, the cavity is conserved in the atomic structure of yeast and human P4-ATPases (Bai *et al.*, 2019; Hiraizumi *et al.*, 2019a; Timcenko *et al.*, 2019a; Nakanishi *et al.*, 2020a, 2020b). The presence of the I(S/R)TTK motif in yeast Dnf1 and Dnf2 and the related ISTAK motif in the human ATP8A2, a homolog of Drs2, suggests that this structural element represents a mechanistic feature conserved in other P4-ATPases (Fig EV3). Using PICT, we assessed the general contribution of the I(S/R)TTK motif in the network of interactions between P4-ATPases and MTCs. Haploid cells expressed MTCs (GARP or TRAPPIII) subunits fused to FRB (bait) and P4-ATPases (Dnf1 or Dnf2) fused to GFP (prey), and when required, DNF1 and DNF2 genes were edited with CRISPR/Cas9. In consonance with a conserved mechanism for the interaction between P4-ATPases and MTCs, mutation of the I(S/R)TTK motif to five alanines weakens significantly all the interactions tested (Fig 5B and EV4D). It is particularly interesting the loss of interaction

between GARP and *dnf1-5A*-GFP and *dnf2-5A*-GFP, whose Interaction score decreased 56.8 and 63.4%, respectively. In agreement with the essential role of GARP in the transport of Dnf1 and Dnf2 to the bud (Takagi *et al.*, 2012; Eising *et al.*, 2019), cells expressing *dnf1-5A*-GFP and *dnf2-5A*-GFP failed to polarize properly the two flippases (Fig EV4E). Thus, our results demonstrate that the I(S/R)TTK motif is required to preserve the overall network, with consequences on the cellular performance of both MTCs and P4-ATPases. To illustrate the biological relevance of such interactions, we further characterized the functional implications of the interaction between Drs2 and TRAPPIII.

Binding to the Drs2 N-terminal tail enhances the function of TRAPPIII

TRAPPIII is in charge of transporting Atg9 from endocytic reservoirs to the Golgi, before Atg9 is delivered to the PAS (Shirahama-Noda *et al.*, 2013). We implemented a microscopy-based system with high-sensitivity and high-temporal resolution to evaluate the relevance of Drs2 binding for the function of TRAPPIII in the transport of Atg9 vesicles (see Materials and Methods). In growing yeast cells,

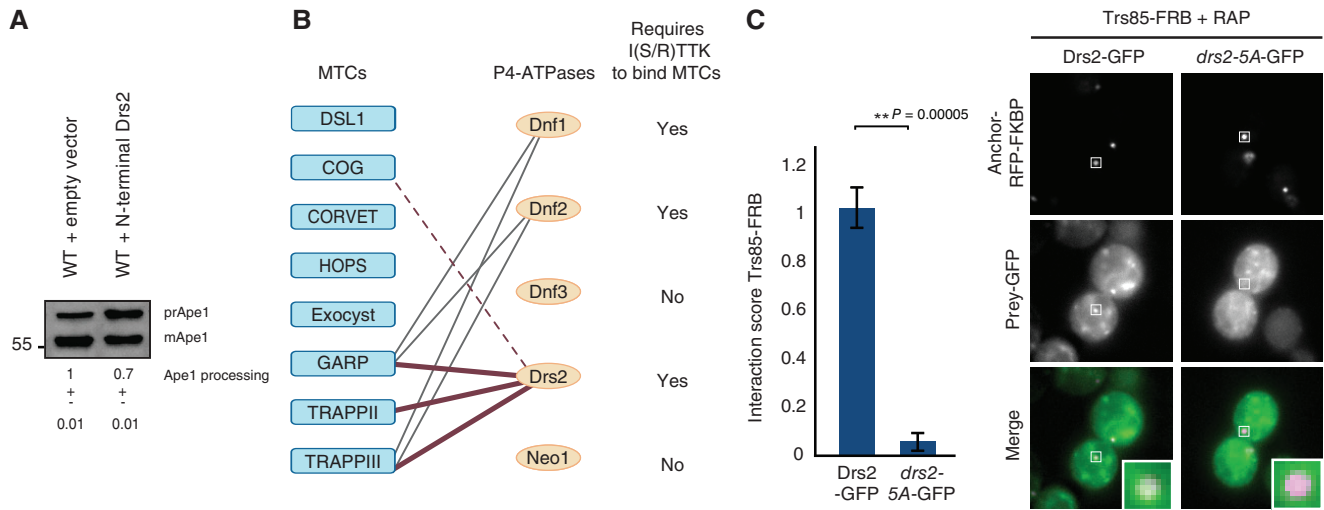


Figure 5. The I(S/R)TTK motif and the interaction between MTCs and P4-ATPases.

- A** Ape1 processing was analyzed by Western blot in cells overexpressing N-terminal Drs2 (1–212 aa) and normalized to the processing achieved in cells with an empty vector \pm SD, $n = 3$.
- B** Network of interactions between MTCs and P4-ATPases (lines) adapted from Fig 1D. XL-MS detected proximal interactions that require the I(S/R)TTK motif (thick maroon lines). The interaction with COG could not be recapitulated by XL-MS (dashed line). P4-ATPases that rely on the I(S/R)TTK motif to bind MTCs are annotated (right column).
- C** Left, PICT assay for the interaction of Trs85-FRB (TRAPPIII) and Drs2-GFP or *drs2-5A*-GFP after adding rapamycin (RAP). The Interaction score was normalized to the measurement of Drs2-GFP. Error bars: mean \pm SD, $n = 3$. Asterisk indicates significant difference as determined by a two-tailed Student's *t*-test (** $P < 0.01$). Right, representative images of the PICT assay. RFP-tagged anchor and GFP-tagged prey are shown in the upper and middle row, respectively. Bottom row shows the merged images. White zoom in boxes, 0.9 μ m. Scale bar, 5 μ m.

Data information: $n =$ biological replicate.

Atg9-GFP can be observed as highly mobile puncta, the vast majority of which correspond to vesicles within the cytoplasm (Yamamoto *et al*, 2012). In agreement with a previous publication (Yamamoto *et al*, 2012), growing wild-type cells present two populations of Atg9 puncta (Fig 6A and Movie EV3). The larger population comprises 86% of the puncta and it is highly mobile (mean speed of 2.3 ± 0.7 nm/ms). The smaller population comprises 14% of the puncta and it has slower mobility (mean speed of 0.7 ± 0.2 nm/ms). Interestingly, in *drs2* Δ and *drs2-5A* cells, the low mobility population increases up to 54% (0.6 ± 0.3 nm/ms) and 50% (0.6 ± 0.2 nm/ms) of the puncta, respectively (Fig 6A and Movies EV4 and EV5). We could not detect Drs2-GFP at the PAS (Fig EV5), suggesting that the I(S/R)TTK motif of Drs2 plays a major role in the trafficking of Atg9 prior to reaching the PAS, most likely in the transport of higher mobility vesicles from lower mobility Atg9 reservoirs. This is further supported by the 39.6% decrease of Atg9-GFP detected at the Ape1-mCherry aggregates upon mutation of the Drs2 I(S/R)TTK motif (Fig 6B). Note that the inability of *drs2-5A* cells of transporting Atg9 to the PAS is likely to be more prominent, because large Ape1 aggregates in mutant cells are more prone to artifactually co-localize with neighboring Atg9 puncta.

Mutation of the I(S/R)TTK motif disrupts the interaction of Drs2 with multiple proteins that contribute to Atg9 transport, such as GARP and TRAPPII subunits (Figs 5B and EV4B). This challenges the interpretation of the Atg9 miss-sorting and the specific contribution that the TRAPPIII-Drs2 interplay might have in this process. We confirmed that the interaction with Drs2 is required for TRAPPIII function with the PICT assay, a technique that provides a good

read-out to measure the capability of proteins to bind membranes *in situ* (Picco *et al*, 2017). We inferred TRAPPIII association with Atg9-loaded membranes by measuring the recruitment of Atg9-GFP to the anchoring platform when using Trs85-FRB as bait. Indeed, the Interaction score between TRAPPIII and Atg9-GFP dropped 84.1% in cells where TRAPPIII could not bind Drs2 (Fig 6C). The partial delivery of Atg9 to the PAS and the residual ability of TRAPPIII to bind Atg9-loaded membranes are in agreement with the observation that the Cvt pathway remains slightly active in *drs2-5A* cells under our experimental conditions (Fig 4D). Vesicle tracking, co-localization and the PICT assay demonstrate that the I(S/R)TTK motif in the Drs2 N-terminal tail strengthens the binding of TRAPPIII on Atg9-loaded membranes and facilitates the delivery of Atg9 for the Cvt pathway.

These results, together with the competition assay and XL-MS experiments (Figs 5A and B and EV4B), uncovered the mechanism used by Drs2 as a regulatory partner of TRAPPIII: Trs85 proximal binding to the Drs2 N-terminal tail stabilizes TRAPPIII on Atg9-loaded membranes, which in turn is necessary for the normal transport of Atg9 from the reservoirs and for the progression of the early stages of the Cvt pathway (Fig 6D).

Discussion

Understanding the mode of action of MTCs requires an approach dedicated to compare side-by-side the mechanistic features of these protein machines. The PICT assay is based on live-cell imaging.

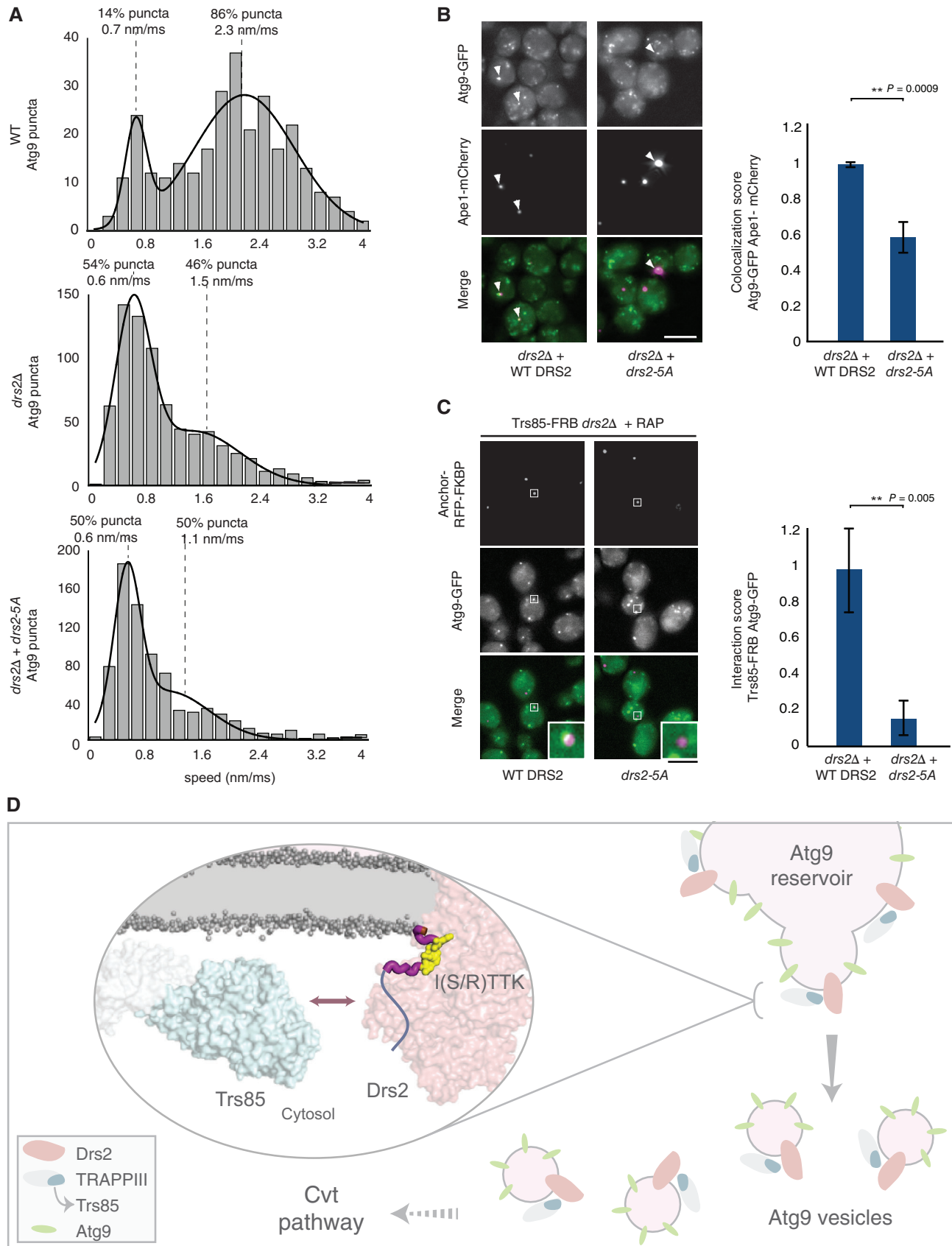


Figure 6.

Figure 6. I(S/R)TTK motif of Drs2 plays a central role in the transport of Atg9.

- A Histograms representing the mean speed of Atg9 puncta observed in wild-type, *drs2Δ* and *drs2-5A* cells. The histograms were fitted to a mixture of Gaussian distributions with two components; the percentage of each population and the means of the fitting curves are indicated on top of the plot.
- B Representative images (left) and quantification (right) of the co-localization between Atg9-GFP and Ape1-mCherry (upper and middle row, respectively) in cells expressing wild-type Drs2 or *drs2-5A*. White arrowheads point to Ape1-mCherry clusters co-localizing with Atg9-GFP.
- C Representative images (left) and quantification (right) of the PICT assay for the interaction of Trs85-FRB (TRAPPIII) and Atg9-GFP in cells expressing wild-type Drs2 or *drs2-5A* after adding rapamycin (RAP). RFP-tagged anchor and GFP-tagged prey are shown in the upper and middle row, respectively. Bottom row shows the merged images. White zoom in boxes, 0.9 μm.
- D Model for the interplay between Drs2 and TRAPPIII.

Data information: B, C Values were normalized to the measurements in cells expressing wild-type Drs2. Error bars: mean ± SD, *n* = 3 biological replicates. Asterisks indicate significant difference as determined by a two-tailed Student's *t*-test (***P* < 0.01). Scale bar, 5 μm.

Thus, PICT provides control of the cellular condition and the functional environment where protein interactions are tested and it overcomes the limitations derived from sample processing. In addition, technical improvements of the method, allowed us to combine genetic interactions and the PICT assay to systematically explore low abundant binding events relevant to the function of MTCs. We found that MTCs localizing at the Golgi recognize P4-ATPases, establishing a network of interactions with unknown biological implications.

To delve into the functional relevance and the molecular mechanism of the interplay between MTCs and P4-ATPases, we analyzed the interaction between TRAPPIII and the lipid flippase Drs2 in the context of Atg9 transport and the Cvt pathway. TRAPPIII is a MTC that controls the transport of Atg9 between reservoirs at the endocytic structures and the Golgi. TRAPPIII is essential so that a small fraction of Atg9 can eventually be delivered to the PAS for the formation of the Cvt vesicle. Drs2 is a lipid flippase that circulates between early endosomes and the TGN. As we could not label Drs2 from different compartments, the PICT technique did not allow us to resolve which subpopulation of Drs2 interacts with TRAPPIII. Nevertheless, given the role of TRAPPIII in transporting Atg9 from endosomes to Golgi (Shirahama-Noda *et al*, 2013), it is plausible that Drs2 and TRAPPIII interact on endosomal structures that serve as Atg9 reservoir. This will need to be clarified in further studies. We show that Drs2 is a regulatory partner of TRAPPIII and provide insight into the mechanism that regulates TRAPPIII function in the Cvt pathway.

As we could not detect Drs2-GFP in the PAS, we reasoned that the Drs2-TRAPPIII assembly is likely not involved in the tethering of Atg9 vesicles at this compartment (Fig EV5). Instead, co-localization and vesicle tracking experiments indicate that Drs2 is critical for the biogenesis of vesicles from the Atg9 reservoirs (Fig 6). In agreement, imaging cellular ultrastructure demonstrated that Drs2 is required for the early stages of the Cvt vesicle biogenesis, before the double-membrane elongates to enwrap the prApe1 cargo (Fig 2E).

Remarkably, both TRAPPIII and Drs2 have been detected on Atg9 vesicles (Kakuta *et al*, 2012; Sawa-Makarska *et al*, 2020), which led us to hypothesize that Drs2 could regulate the recruitment of TRAPPIII on Atg9-loaded membranes. Trs85 is the sole specific subunit of TRAPPIII and it is thought to be responsible for directing the complex to the target membrane (Lynch-Day *et al*, 2010). Recent structural analysis showed that the Trs85 subunit binds membranes through a positively charged amphipathic helix, an interaction that is required for TRAPPIII function in nonselective autophagy and the

secretory pathway (Galindo *et al*, 2021; Joiner *et al*, 2021). Thus, a possibility would be that Drs2 accumulated negatively charged PS at the cytosolic leaflet of Atg9 compartments and that, in turn, PS stabilized TRAPPIII through interactions with positive charges of the Trs85 amphipathic helix. This mechanism is appealing as it would offer a mechanistic link between the activity of the lipid flippase (Drs2) and the lipid scramblase (Atg9). However, electrostatic interactions between PS and Trs85 amphipathic helix on the surface of Atg9 vesicles are not necessary for the Cvt pathway as cells that cannot synthesize PS process Ape1 normally (Fig 3D). Genetics confirmed this observation and showed that Drs2 role in the Cvt pathway is independent of the molecular functions that had been previously described for the lipid flippase.

It has also been postulated that TRAPPIII might be stabilized on the surface of specific membranes through protein–protein interactions with Trs85 (Galindo *et al*, 2021; Joiner *et al*, 2021). Noteworthy, when the environmental temperature becomes colder, the relevance of Drs2 in the Cvt pathway increases concomitantly to the levels of Drs2-Trs85 binding (Figs 2A and C and EV2), supporting that the function of Drs2 in this process is mediated by the interaction with Trs85. In agreement, a competition assay underscores that protein–protein interactions with the Drs2 N-terminal tail are central for the Cvt pathway.

The lack of structural information of Drs2 N-terminal tail complicates structure–function analysis. However, we identified a conserved I(S/R)TTK motif nested in a cavity of the N-terminal tail of the flippase that is required for the role of Drs2 in the Cvt pathway. We used mutagenesis and XL-MS to show that TRAPPIII binds Drs2 through Trs85 subunit via a direct or close proximity interaction that relies on the I(S/R)TTK motif. Note that in the XL-MS experiments, we used a partial cross-linking with DSSO, a crosslinker that is 10 Å in length, to minimize the detection of indirect protein–protein interactions. Indeed, as the XL-MS dataset does not report full complexes but specific subunits of GARP, TRAPPII, and TRAPPIII, this implies that our XL-MS approach detected none or marginal indirect interactions. In addition, XL-MS further stresses the central role of Drs2 in Atg9 homeostasis, as the mutation of Drs2 I(S/R)TTK motif hinders the binding to six proteins that bind Atg9: Trs85, Vps17, Pep1, Vps45, Akr1, and Vti1, the last two being components of the Atg9 vesicle too (Fig EV4B; Sawa-Makarska *et al*, 2020).

Multiple evidences indicate that the function of Drs2 in the Cvt pathway is subjected to a regulatory mechanism that remains elusive: the cell modulates the role of Drs2 in the Cvt pathway in response to thermal fluctuations (i.e., while Drs2 is required to

maintain the Cvt pathway functional under mild (30°C) and cold ($\leq 23^\circ\text{C}$) environments, at higher temperatures (37°C) the flippase is nearly dispensable; Fig 2A and EV2A). Drs2 contribution to Ape1 processing is also sensitive to nutrient availability (i.e., while mApe1 is hardly detected in $\Delta drs2$ cells in rich media, Ape1 processing defect in starving $\Delta drs2$ cells, when bulk autophagy is activated, is minor; Fig EV2E). In consonance, a former study showed that Drs2 is not required for the processing of Ape1 at the stationary phase (Wang et al, 2017), confirming that Drs2 function is controlled according to different cellular stimuli. Indeed, Drs2 activity is regulated by multiple interactions. The small GTPase Arl1 binds within the N-terminal unstructured region of Drs2 and serves to stimulate Drs2 flippase activity (Tsai et al, 2013). Drs2 is autoinhibited by its C-terminal tail and interactions with PI4P and Gea2 in the C-terminal region, along with Arl1 at the N-terminus, serve to displace the autoinhibitory domain and activate Drs2 (Chantalat, 2004; Natarajan et al, 2004; Zhou et al, 2013; Timcenko et al, 2019a). Investigating the relevance of these interactions in opening up the I (S/R)TTK motif for binding to Trs85 might shed light on the mechanism that controls Drs2 role in the Cvt.

Structural analysis on the reconstituted Drs2-TRAPPIII assembly will be required to decipher the binding interface between Drs2 and Trs85 on Atg9-loaded membranes and how this interaction is regulated by different cellular stimuli. Nonetheless, we provide molecular insight that allows us to discuss a possible regulatory mechanism. Recent structural analysis of human ATP8A1 showed that the cavity is momentarily opened in the transition between the E2P and E2Pi-PL states along the lipid translocation cycle. During this rearrangement, the neck of the cavity switches from a closed conformation of 14.1 Å to an open conformation of 20.6 Å (Cys50-to-Asn60; Hiraizumi et al, 2019a). This allows us to speculate that similar conformational dynamics, which would expose the I(S/R)TTK motif, might act as a structural switch to regulate the assembly of Drs2 and TRAPPIII and the role of the flippase in the Cvt pathway. According to this hypothesis, although PS flipping is not required for the Cvt pathway, perturbing the cycling between Drs2 states should hamper Ape1 processing. Indeed, cells expressing a mutant form of Drs2 that cannot cycle normally through E2P (D560N, which is a dead mutant) only manages to process about 50% of Ape1 (Fig 3C).

We also provide mechanistic insight into the interplay between P4-ATPases and the MTCs. MTCs base their mechanism of action on protein-protein interactions with other components of the trafficking machinery such as GTPases, SNAREs, and SM proteins. For instance, the COG complex interacts with the Rab GTPase Ypt1 to function within the Golgi (Suvorova et al, 2002) while the GARP complex cooperates with the Rab GTPase Ypt6 in tethering endosome-derived vesicles to the TGN (Siniosoglou & Pelham, 2001). In this study, we reveal that binding to P4-ATPases is a common feature shared by MTCs controlling vesicle transport at the Golgi and that these interactions require the I(S/R)TTK motif nested in the N-terminal cavity of P4-ATPases. GARP, for instance, is known to be necessary for the recycling of Dnf1 and Dnf2 and the function of these flippases at the plasma membrane (Takagi et al, 2012; Eising et al, 2019). The PICT assay and the subcellular distribution of *dnf1-5A-GFP* and *dnf2-5A-GFP* suggest that the I(S/R)TTK motif allows GARP to bind and transport Dnf1 and Dnf2 during their recycling. Further analysis of the interplay between P4-ATPases and

MTCs will open novel avenues for understanding the functional relevance of these interactions and their implications in vesicle trafficking. For example, the role of TRAPPIII in the secretory pathway stresses the need to characterize the function of the Drs2-TRAPPIII interaction in the transport of COPII vesicles.

Overall, MTCs are protein complexes with essential roles in multiple cellular processes, including autophagy, cell polarity, pathogen infection, and protein glycosylation, just to give some examples (Zuo et al, 2009; Bröcker et al, 2010; Shirahama-Noda et al, 2013; Schou et al, 2014). Thus, binding to P4-ATPases arises as a critical mechanism to understand MTCs mechanism of action, with implications that likely go beyond the transport of Atg9 and the Cvt pathway.

Materials and Methods

Yeast strains, plasmids, and cultures

Saccharomyces cerevisiae (*S. cerevisiae*) strains are derivatives of BY4741 or BY4742 backgrounds. Strains with genes coding for C-terminal tags, deleted genes, and/or mutated alleles were generated by homologous recombination following standard PCR strategies (Janke et al, 2004). OGY1015 and OGY1016 strains were generated following CRISPR-Cas9 technology as described by Laughery et al, 2015. Those strains harboring exogenous genes coded in plasmids were generated by transformation. All Drs2 constructs were expressed from a plasmid using the DRS2 promoter except for those plasmids in Fig 5A, which use GAL1 promoter. All strains are listed in Datasets EV1–EV4. All plasmids used are listed in Table EV1.

Strains used for the PICT assay express the anchor Tub4-RFP-FKBP and harbor different combinations of baits (FRB fusions at the C-terminus) and preys (GFP fusions at the C-terminus; see Datasets EV1–EV3; Torreira et al, 2017). Parental cells expressing the anchor Tub4-RFP-FKBP and a bait-FRB were constructed on the OGY0307 genetic background. Parental cells expressing the prey-GFP were constructed in the BY4741 genetic background or obtained from the genomic C-terminal GFP fusion collection (ThermoFisher). Excluding those strains harboring plasmids that code for Drs2-GFP and *drs2-5A-GFP*, the PICT experiments were carried out with yeast strains constructed with the SGA approach (Tong & Boone, 2005).

Yeast cells were grown in YPD liquid medium at 30°C and 220 rpm until saturation (≈ 16 h). Cells harboring plasmids were grown in synthetic minimal liquid medium lacking the amino acid of choice. In experiments with *cho1Δ* cells, the medium was supplemented with 1 mM Ethanolamine. After reaching saturation, cells were diluted to an optical density of $\text{OD}_{600} = 0.2$ in the medium of interest and cultured at 30°C and 220 rpm until they reached an early logarithmic phase ($\text{OD}_{600} \approx 1$) (experiments Fig 1). Unless indicated, in the rest of experiments cells were then incubated at 23 or 37°C for 2 h before performing the experiment.

Imaging

After saturation in the YPD culture, cells were diluted and grown in Low Flo medium (Yeast Nitrogen Base Low Fluorescence without Amino acids, Folic Acid and Riboflavin, 2% Synthetic complete

Mixture Drop-out lacking essential amino acids as required and 2% glucose). When they reached an early logarithmic phase ($OD_{600} \approx 1$), cells were attached to Concanavalin A (0.1 $\mu\text{g/ml}$)-coated glass bottom plates. When required, 10 μM of rapamycin was added 20–30 min before imaging. Images in Figs 1, 2B, 5B and EV1 and Movie EV1 were acquired on a ScanR (Olympus) microscope based on a IX81 stand, equipped with 100 \times /1.40 objective lens, an Orca-ER camera (Hamamatsu), a MT20 Xenon arc lamp illumination system holding excitation filter and two complete fluorescence filter cubes from AHF respectively optimized for GFP (ET Bandpass 470/40 + Beamsplitter 500 DVXRUV + ET Bandpass 525/50) and RFP (ET Bandpass 545/30 + Beamsplitter 580 DVXRUV + BrightLine HC 617/73). Images in Figs 6B and EV4A and Movie EV2, were acquired on a Nikon ECLIPSE Ti2-E inverted microscope equipped with a 100 \times /1.49 SR TIRF objective (Nikon), a sCMOS Zyla 4.2 Andor camera and a SpectraX Lumencore LED system with two fluorescence filter cubes (Semrock) optimized for GFP (LF488-C) and LED-mCherry. Images in Figs 5C and EV4C–E were acquired with the same Nikon ECLIPSE Ti2-E inverted microscope and SpectraX Lumencore LED system but with a PRIME 95b camera. For the PICT experiments shown in Figs 1B and D and EV1 and the screening among MTCs and P4-ATPases of Fig 5B automated imaging acquisition was carried out. The acquisition software (ScanR, Olympus) was set up to detect those cells' planes with the highest RFP signal. This provided a focal plane that captured the highest number of anchoring platforms in focus. Images were obtained sequentially by switching the filter cubes. Strains were imaged in the RFP (200 ms) and GFP channels (200 and 1,500 ms in Fig 1B; 200 and 1,000 ms in Fig 1D) and each strain was imaged in at least six fields of view. In PICT experiments in Figs 1C and 2C and for the imaging in Fig 2B and in Movie EV1 cells were imaged using Xcellence (Olympus) as acquisition software. For the PICT experiments in Fig 5C and EV4C–E, cells were imaged using Micro-Manager (Edelstein et al, 2010) as acquisition software. For the co-localization assay in Fig 6B, in PICT experiments in Figs 6C and EV4A and in Movie EV2, cells were imaged using NIS-Elements as acquisition software. In experiments in Figs 1C, 2B and C, 5B, 6B and C, and EV1, strains were imaged in brightfield and in the RFP (200 ms) and/or the GFP (exposition time was optimized manually) channels. In experiments of Fig 5C and EV4C–E, strains were imaged in the RFP (100 ms) and/or the GFP (1,000 ms) channels. For Movies EV3–EV5, see Vesicle tracking section.

Protein interactions from imaging complexes after translocation (PICT)

PICT technique allows the quantitative characterization of protein interactions *in vivo*. The addition of rapamycin to culture media induces FRB-FKBP heterodimerization and translocation of the protein tagged to FRB (bait-FRB) to anchoring platforms engineered in the cell by tagging an anchoring molecule to RFP and FKBP (anchor-RFP-FKBP). GFP-tagged proteins (prey-GFP) that are bound to the bait-FRB are co-translocated to these anchoring platforms. These changes in localization can be subsequently quantified using dual-color live-cell imaging. Recently, we increased PICT sensitivity up to 200-fold. We designed a new anchoring platform by tagging Tub4, a component of the spindle pole body, with RFP and FKBP (Tub4-RFP-FKBP). The resulting cells harbor one or two

anchoring platforms only. Thus, even low abundant complexes accumulate enough prey-GFP in each of these anchoring platforms to be efficiently detected and quantified (Torreira et al, 2017). All PICT experiments were performed in rapamycin-insensitive strains carrying the *tor1-1* mutation in the TOR1 gene and where the endogenous FPR1 gene was deleted (Gallego et al, 2013). Images were taken prior and after rapamycin addition.

Selection of proteins for the protein–protein interaction screen

First, we identified the bait-FRBs of each MTC that allows anchoring more efficiently the fully assembled complex (Fig 1A and Dataset EV2). For each MTC, we generated a set of strains expressing all possible combinations of subunits tagged to FRB and GFP. Then, we selected the corresponding bait-FRB that showed highest Interaction score for the other subunit of the corresponding complex.

Second, we used genetic interactions to select the prey-GFPs for the screen. *S. cerevisiae* has eight MTC complexes, each of them with a different protein composition. Genes coding for MTC subunits (MTC Gene or GM) interact genetically with 1,283 genes (Candidate Genes or CG) in yeast from the Saccharomyces Genome Database in 2013 (Stark et al, 2006; Data ref: Stark et al, 2006). In total, *S. cerevisiae* has 5,820 genes.

For each Candidate and MTC Gene pair CG_i-GM_j , we calculated its pairwise interaction probability P_{ij} given by:

$$P_{ij} = PC_{ij} * PM_{ji},$$

where PC_{ij} is the probability that a Candidate Gene i interacts with MTC Gene j ; and PM_{ji} is the probability that MTC Gene j interacts with Candidate Gene i .

When a Candidate Gene i interacts genetically with a set J of subunits of a given MTC, we use a genetic score S_i defined as

$$S_i = \prod_{j \in J} P_{ij},$$

to measure the probability of measuring randomly the genetic interaction profile with Candidate Gene i .

Six hundred and seventy-six Candidate Genes with a “Genetic Interaction score” $< 10^{-6}$ were selected for further analysis. We then selected the corresponding 426 prey proteins that are included in the yeast C-terminally GFP-tagged genomic collection (Huh et al, 2003) and whose binding to MTC subunits had not been described at the time of the screening (Dataset EV1).

Image analysis

A custom image analysis workflow was implemented as an ImageJ (<http://rsb.info.nih.gov/ij/>) macro to automate operations and process whole data sets. Essentially, this workflow aimed to estimate the co-localization (overlap) between spots independently segmented in the images from RFP (anchors) and GFP (preys) channels.

To exclude out of focus (or empty) images, a sharpness factor was first computed (standard deviation of the image intensity normalized to its mean intensity in RFP channel). The fields of view

with sharpness factor above a user defined threshold were processed by the following sequence of operations aiming to segment bright spots: (i) smoothing; (ii) background subtraction; (iii) local thresholding; (iv) median filtering; and (v) discard small particles below a certain area. For each experimental condition, the functional parameters of the workflow were manually optimized to lead to the best results.

The area of overlap between preys and anchors was then estimated by counting the number of foreground pixels common in both segmentation masks (logical AND operation). This area was then normalized to the count of foreground pixels in the RFP segmentation mask (anchors area) to lead to the *fractional anchor to prey overlap* F_o . Next, the mean intensity I_o from the GFP channel was estimated inside the regions of spot overlap and the weighted average of F_o . I_o was computed over the whole field of view (anchors area used for weighting).

Analysis of PICT experiments

In the primary selection of positive hits (screening of Fig 1B), a Fold change was estimated for each condition as the ratio between the weighted average of F_o . I_o after and prior to rapamycin addition (see Fold change values in Dataset EV1). An arbitrary Fold change of 3 was established as potential interactions. This primary list was manually curated and confirmed in one-to-one PICT experiments.

We defined an Interaction score as the subtraction of the weighted average of F_o . I_o prior to rapamycin addition from the weighted average of F_o . I_o upon rapamycin addition. In PICT experiments conducted to determine the most efficient baits used to anchor each MTC (Fig 1A and Dataset EV2) and to evaluate the network of interactions between P4-ATPases and MTCs (Fig 1D and Dataset EV3), an arbitrary Interaction score of 100 was established to identify positive interactions. This primary list was manually validated. All one-to-one PICT experiments (Figs 2C, 5C, 6C and EV4C and E) were done in at least three biological replicates. For the statistical analysis, the Interaction score of one-to-one experiments was normalized to the measurement of those strains expressing wild-type Drs2 (Figs 5C, 6C and EV4E), wild-type Dnf1 or Dnf2 (Fig EV4C) or to the measurement of those strains after 2 h at 23°C (Fig 2C).

Co-localization assays

Similar as described above, the co-localization score S_o was determined as the area of overlap between GFP and RFP channels estimated by counting the number of foreground pixels common in both segmentation masks (logical AND operation) over all fields of view (RFP or GFP area used for weighting in Figs 6B and EV4A, respectively). For the statistical analysis, the co-localization score was estimated in cells harboring wild-type Drs2 or *drs2-5A* and normalized to the measurement of those strains expressing wild-type Drs2.

In Movies EV1 and EV2, cells grown in YPD were labeled with 8 μ M FM4-64. Prior to imaging, cells were kept in the dark for 30 min to stain the vacuole. Then, cells were washed twice with Low Flo liquid medium to remove YPD and free FM4-64 before imaging. Imaris software was used to obtain the 3D reconstruction of yeast cells imaged with Z-stacks of 250 nm step in size.

Vesicle tracking

The protocol used for the tracking of Atg9 vesicles is based on the method reported previously (Yamamoto *et al*, 2012). Atg9 was C-terminally fused to a 3xGFP tag. The best focal plane was selected for imaging and 2D time-lapses were acquired at 20 frames per second with a 488 nm laser excitation providing a power of approximately 50 mW at the back aperture of the objective lens, placed on an inverted microscope (IX71 Olympus) optimized for oblique illumination and fast acquisition (Hamamatsu Flash4 v2 sCMOS camera) with a 100 \times /1.45 objective lens. Oblique illumination reduces background signal and the high-speed camera allows high-temporal resolution. The axial extension of the laser inclined sheet was approximately 1.5–2 μ m and the usable field of view approximately 40 \times 40 μ m; images were cropped to increase acquisition speed and illumination was kept continuous during the time-lapses. More than 290 trajectories of GFP puncta were collected from several time-lapses for each strain.

The images were compensated for bleaching by applying the correction method “Exponential fit” from ImageJ “Bleach Correction” plugin. Individual vesicles were then identified and tracked by ImageJ TrackMate plugin (Tinevez *et al*, 2017). The tracks were linked with “simple LAP” option, a maximal linking distance of 5 pixels and no gap-closing allowed. Finally, only tracks containing a minimum of 5 spots were kept to discard spurious tracks.

For each time-lapse, the average speed of the vesicles was computed within tracks and binned to a 20bin histogram spanning from 0 to 200 nm/frame. The resulting histograms were fitted to a two-component Gaussian mixture model (GMM). The fits were optimized by the nonlinear least-squares regression (MATLAB). From these models, we estimated the mean speed (and standard deviation) for both populations. The fraction of spots belonging to each population was derived as the fractional areas below each Gaussian component normalized to the area below the fitted curve.

Electron microscopy (EM) and correlative light and electron microscopy (CLEM)

Cells were grown as described before. High-pressure freezing, freeze-substitution, and embedding in EM and CLEM experiments were performed as described in the literature (Müller-Reichert, 2012). In brief, yeast cells were pelleted and the yeast paste was loaded into 200 μ m depth planchettes and high-pressure frozen using the High Pressure Freezing Leica EM ICE. The planchette sandwich was disassembled under liquid nitrogen prior to freeze-substitution. Samples were freeze-substituted using a temperature-controlling AFS2 (Leica) with an FPS robot.

EM pictures were then taken at various magnifications in a JEOL JEM 1011 electron microscope equipped with a Veleta 2 k \times 2 k side-mounted TEM CCD camera (Olympus).

For CLEM experiments, samples were stored protected from light after polymerization and processed further within 2 days. Ultrathin sections were cut with a diamond knife in a microtome (Leica EM UC7) and picked up on carbon-coated 200 mesh copper grids. Fluorescent fiducial markers, 0.02 μ m Blue Fluospheres (Molecular Probes; excitation 365 nm/emission 415 nm) were adhered to the section. Then, grids were placed section-face down onto a 15 μ l drop of Fluospheres for 10 min, blotted with filter paper and

washed with three drops of water with blotting between the washing steps. To minimize bleaching, fluorescence images were taken with an IX83 (Olympus) during the next 3 days. From 2 to 5 images were taken in different focal planes for both channels (GFP and blue fluorescent fiducials). During imaging, the positions on the grid of the imaged areas of interest were recorded. EM pictures of recorded positions were taken and correlated to the corresponding GFP images. To estimate the fraction of cells that present Ape1-GFP aggregates in our images, we analyzed 660 cells (from five sections) from which we detected Ape1-GFP aggregates in 2% of the cells. In total, we analyzed at higher magnification 58 Ape1-GFP aggregates by CLEM.

Immunoblot analysis

In experiments of Figs 2A, 3A and C–E, 4D and EV2, cells were grown as described before. In experiment of Fig 5A cells were grown overnight at 30°C in synthetic minimal liquid medium lacking Uracil and supplemented with 2% galactose to induce overexpression. Next morning, with an optical density (OD) close to 0.5, cultures were left at 23°C for 2 h. In Fig EV2, cultures were left as describe in the figure legend.

An alkaline extraction method described by Kushnirov (2000) was followed to prepare the samples for Western blot analysis. The blocking step was done with 5% milk powder in TBS-0.5% Tween 20 for 1 h at room temperature. Incubation with primary anti-Ape1 antibody was performed overnight at 4°C (1:4,000 antibody dilution in blocking solution). Incubation with secondary anti-rabbit antibody was performed for 1 h at room temperature (1:2,500 antibody dilution in blocking solution).

Western blot quantification was carried out with the ImageStudio™ Lite software. In the exported data, the background of the prApe1 and mApe1 bands' signal intensities is automatically corrected from a region right under or above the band. To calculate the Ape1 processing, the % mApe1 for each strain was calculated and normalized by the % mApe1 achieved in wild-type cells. To calculate the % mApe1, the signal intensity of mApe1 multiplied by its band area was divided by the result of the addition of the signal intensities of prApe1 and mApe1, each one multiplied by its corresponding band area. In experiment of Fig 3A, the triplicates of wild-type cells at 23°C from Fig 2A were used to normalize the % mApe1 achieved in each of the strain analyzed.

Cross-linking and immunoprecipitation

Cells were grown as described before. 600 OD₆₀₀ units of yeast cells were washed twice with B88 buffer (19.97 mM HEPES pH = 6.8, 149.77 mM KOAc, 250.32 mM sorbitol, 4 mM MgOAc). Cell lysis was performed using Freezer/Mill® Cryogenic Grinder (Spex® SamplePrep, model 6775). Cell powder was resuspended in 5 ml B88 + PMSF + protein inhibitor and centrifuged at 3000 rpm for 10 min to eliminate cell debris. The supernatant was taken and DSSO was added to a final concentration of 2.5 mM. After 20 min, 0.5 M glycine was added to stop the reaction. The mix was incubated for 5 min. Triton X-100 was added to a final concentration of 1%. The suspension was incubated with rotation for 1 h at 4°C before removing the insoluble components by 13,000 rpm centrifugation at 4°C during 1 h. For the immunoprecipitation, the samples were

incubated for 1 h with previously equilibrated Bab agarose beads (Chromotek) at 4°C. Then, they were incubated with GFP-Trap_Agarose (Chromotek) overnight at 4°C. The resin was first washed four times with a solution containing 8 M urea, 2 M NaCl and 1% TX-100 in PBS, and it was subsequently washed four more times with PBS.

The resin used in immunoprecipitation was cleaned three times with 500 µl of 200 mM ammonium bicarbonate and 60 µl of 6 M urea/200 mM ammonium bicarbonate were added. Samples were then reduced with dithiothreitol (30 nmol, 37°C, 60 min), alkylated in the dark with iodoacetamide (60 nmol, 25°C, 30 min) and diluted to 1 M urea with 200 mM ammonium bicarbonate for trypsin digestion (1 µg, 37°C, 8 h, Promega cat # V5113).

After digestion, peptide mix was acidified with formic acid and desalted with a MicroSpin C18 column (The Nest Group, Inc) prior to LC-MS/MS analysis.

Chromatographic and mass spectrometric analysis

Samples were analyzed using an LTQ-Orbitrap Velos Pro mass spectrometer (Thermo Fisher Scientific, San Jose, CA, USA) coupled to an EASY-nLC 1000 (Thermo Fisher Scientific (Proxeon), Odense, Denmark). Peptides were loaded onto the 2-cm Nano Trap column with an inner diameter of 100 µm packed with C18 particles of 5 µm particle size (Thermo Fisher Scientific) and were separated by reversed-phase chromatography using a 25-cm column with an inner diameter of 75 µm, packed with 1.9 µm C18 particles (Nikkyo Technos Co., Ltd., Japan). Chromatographic gradients started at 93% buffer A and 7% buffer B with a flow rate of 250 nl/min for 5 min and gradually increased 65% buffer A and 35% buffer B in 60 min. After each analysis, the column was washed for 15 min with 10% buffer A and 90% buffer B. Buffer A: 0.1% formic acid in water. Buffer B: 0.1% formic acid in acetonitrile.

The mass spectrometer was operated in positive ionization mode with nanospray voltage set at 2.1 kV and source temperature at 300°C. Ultramark 1621 was used for external calibration of the FT mass analyzer prior the analyses, and an internal calibration was performed using the background polysiloxane ion signal at m/z 445.1200. The acquisition was performed in data-dependent acquisition (DDA) mode and full MS scans with 1 microscans at resolution of 60,000 were used over a mass range of m/z 350–2,000 with detection in the Orbitrap. Auto gain control (AGC) was set to 1E6, dynamic exclusion (60 s) and charge state filtering disqualifying singly charged peptides was activated. In each cycle of DDA analysis, following each survey scan, the top 20 most intense ions with multiple charged ions above a threshold ion count of 5,000 were selected for fragmentation. Fragment ion spectra were produced via collision-induced dissociation (CID) at normalized collision energy of 35% and they were acquired in the ion trap mass analyzer. AGC was set to 1E4, isolation window of 2.0 m/z , an activation time of 10 ms and a maximum injection time of 100 ms were used. All data were acquired with the Xcalibur software v2.2.

Digested bovine serum albumin (New England Biolabs cat # P8108S) was analyzed between each sample to avoid sample carry-over and to assure stability of the instrument and QCloud (Chiva et al, 2018) has been used to control instrument longitudinal performance during the project.

Mass spectrometric data analysis

Acquired spectra were analyzed using the Proteome Discoverer software suite (v1.4, Thermo Fisher Scientific) and the Mascot search engine (v2.6, Matrix Science; Perkins *et al*, 1999). The data were searched against a SGD, 6080 entries (Data ref: Saccharomyces Genome Database, 2016) plus a list (Beer *et al*, 2017) of common contaminants and all the corresponding decoy entries. For peptide identification, a precursor ion mass tolerance of 7 ppm was used for MS1 level, trypsin was chosen as enzyme and up to three missed cleavages were allowed. The fragment ion mass tolerance was set to 0.5 Da for MS2 spectra. Oxidation of methionine and N-terminal protein acetylation were used as variable modifications, whereas carbamidomethylation on cysteines was set as a fixed modification. False discovery rate (FDR) in peptide identification was set to a maximum of 5%. PSM were normalized by the median of Drs2 PSM.

SAINTexpress algorithm was used to score protein–protein interactions (Guoci Teo *et al*, 2014).

Structural modeling

Protein flippases Dnf1, Dnf2, Dnf3 and Neo1 were modeled using Modeler from the HHSearch server (Zimmermann *et al*, 2018), using Drs2 as a template (PDB ID: 6ROH:A) (Timcenko *et al*, 2019a; Data ref: Timcenko *et al*, 2019b). The ATP8A2 homology model was obtained with Modeler from the HHSearch server (Zimmermann *et al*, 2018), using ATP8A1 as template (PDB ID: 6K7N). To model Drs2 within the membrane we used the data from the MemProtMD database (Newport *et al*, 2019). Images were generated using PyMOL (The PyMOL Molecular Graphics System, Version 2.3.4 Schrödinger, LLC.).

Gene ontology enrichment analysis

The *P*-value (*P*) for the Gene Ontology enrichment was calculated using the Hypergeometric distribution corrected by the Bonferroni method of multiple test correction.

Data availability

The mass spectrometry proteomics data have been deposited to the ProteomeXchange Consortium via the PRIDE (Perez-Riverol *et al*, 2022) partner repository with the dataset identifier PXD038527 (<https://www.ebi.ac.uk/pride/archive/projects/PXD038527>).

Expanded View for this article is available [online](#).

Acknowledgments

OG was funded by research grants from the Spanish funding agency (PGC2018-095745-B-I00, EUR2019-103815 and PID2021-127773NB-I00/FEDER UE and supported by the “Unidad de Excelencia María de Maeztu” (ref: MDM-2014-0370) funded by the MCIN/AEI/10.13039/501100011033) and a Research Grant from HFSP (ref: RGP0017/2020). The proteomics analyses were performed in the CRG/UPF Proteomics Unit which is part of the Proteored, PRB3 and is supported by grant PT17/0019, of the PE I + D + i 2013–2016, funded by ISCIII and ERDF. We thank Josep Vilardell, Bernat Crosas, Amy Curwin, Vivek Malhotra,

Michael Knop, Marko Kaksonen, Kenji Maeda, Manuel García-Muñiz and Charles Boone for providing devices, reagents, strains and plasmids. We thank the Advanced Digital Microscopy Core Facility (ADMCF), the Biostatistics/Bioinformatics and the Mass Spectrometry and Proteomics facilities of the IRB Barcelona for live-cell imaging, technical support and also sharing devices with us. We thank Simona Barankova, Radovan Dojilovic and Daniel Castaño-Díez for fruitful discussions. We thank Raúl Méndez and Ignasi Fita for their support and mentoring during these years. IP was supported by FPI awarded by the Spanish Ministry of Economy and Competitiveness (MINECO) (ref: BES-2013-063945) and EMBO Short-Term Fellowship 7076.

Author contributions

Irene Pazos: Conceptualization; formal analysis; investigation; methodology; writing – original draft; writing – review and editing. **Marta Puig-Tintó:** Investigation; methodology; writing – review and editing. **Laura Betancur:** Investigation; methodology; writing – review and editing. **Jorge Cordero:** Investigation; methodology; writing – review and editing. **Nereida Jiménez-Menéndez:** Investigation; methodology; writing – review and editing. **Marc Abella:** Investigation; methodology; writing – review and editing. **Altair C Hernández:** Investigation; methodology; writing – review and editing. **Ana G Duran:** Investigation; methodology; writing – review and editing. **Emi Adachi-Fernández:** Investigation; writing – review and editing. **Carla Belmonte-Mateos:** Investigation; writing – review and editing. **Susana Sabido-Bozo:** Resources; methodology. **Sébastien Tosi:** Data curation; software; formal analysis; writing – review and editing. **Akiko Nezu:** Resources; methodology. **Baldomero Oliva:** Formal analysis; supervision; methodology; writing – review and editing. **Julien Colombelli:** Software; methodology; writing – review and editing. **Todd R Graham:** Conceptualization; resources; writing – review and editing. **Tamotsu Yoshimori:** Resources; writing – review and editing. **Manuel Muñiz:** Resources; methodology; writing – review and editing. **Maho Hama-saki:** Conceptualization; resources; methodology; writing – review and editing. **Oriol Gallego:** Conceptualization; formal analysis; supervision; funding acquisition; investigation; writing – original draft; writing – review and editing.

Disclosure and competing interests statement

The authors declare that they have no conflict of interest.

References

- Alder-Baerens N, Lisman Q, Luong L, Pomorski T, HJ CM (2006) Loss of P4 ATPases Drs2p and Dnf3p disrupts aminophospholipid transport and asymmetry in yeast post-Golgi secretory vesicles. *Mol Biol Cell* 17: 1632–1642
- Baba M, Osumi M, Scott SV, Klionsky DJ, Ohsumi Y (1997) Two distinct pathways for targeting proteins from the cytoplasm to the vacuole/lysosome. *J Cell Biol* 139: 1687–1695
- Bai L, Kovach A, You Q, Hsu HC, Zhao G, Li H (2019) Autoinhibition and activation mechanisms of the eukaryotic lipid flippase Drs2p-Cdc50p. *Nat Commun* 10: 1–10
- Balderhaar HJ, Ungermann C (2013) CORVET and HOPS tethering complexes – coordinators of endosome and lysosome fusion. *J Cell Sci* 126: 1307–1316
- Balderhaar HJK, Lachmann J, Yavavli E, Bröcker C, Lürick A, Ungermann C (2013) The CORVET complex promotes tethering and fusion of Rab5/Vps21-positive membranes. *Proc Natl Acad Sci USA* 110: 3823–3828
- Beer LA, Liu P, Ky B, Barnhart KT, Speicher DW (2017) Efficient quantitative comparisons of plasma proteomes using label-free analysis with MaxQuant. *Methods Mol Biol* 1619: 339–352

- Bröcker C, Engelbrecht-Vandré S, Ungermann C (2010) Multisubunit tethering complexes and their role in membrane fusion. *Curr Biol* 20: 943–952
- Chantalat S (2004) The Arf activator Gea2p and the P-type ATPase Drs2p interact at the Golgi in *Saccharomyces cerevisiae*. *J Cell Sci* 117: 711–722
- Chen J, Zheng XF, Brown EJ, Schreiber SL (1995) Identification of an 11-kDa FKBP12-rapamycin-binding domain within the 289-kDa FKBP12-rapamycin-associated protein and characterization of a critical serine residue. *Proc Natl Acad Sci USA* 92: 4947–4951
- Chen C-Y, Ingram MF, Rosal PH, Graham TR (1999) Role for Drs2p, a P-type ATPase and potential aminophospholipid translocase, in yeast late Golgi function. *J Cell Biol* 147: 1223–1236
- Chiva C, Olivella R, Borràs E, Espadas G, Pastor O, Solé A, Sabidó E (2018) QCloud: a cloud-based quality control system for mass spectrometry-based proteomics laboratories. *PLoS One* 13: 1–14
- Choi HS, Han GS, Carman GM (2010) Phosphorylation of yeast phosphatidylserine synthase by protein kinase a: identification of SER46 and SER47 as major sites of phosphorylation. *J Biol Chem* 285: 11526–11536
- Conibear E, Cleck JN, Stevens TH (2002) Vps51p mediates the association of the GARP (Vps52/53/54) complex with the late Golgi t-SNARE Tlg1p. *Mol Biol Cell* 21: 1610–1623
- Costanzo M, Baryshnikova A, Myers C L, Andrews B, Boone C (2011) Charting the genetic interaction map of a cell. *Curr Opin Biotechnol* 22: 66–74
- Dubuke ML, Munson M (2016) The secret life of tethers: the role of tethering factors in SNARE complex regulation. *Front Cell Dev Biol* 4: 1–8
- Edelstein A, Amodaj N, Hoover K, Vale R, Stuurman N (2010) Computer control of microscopes using µManager. *Curr Protoc Mol Biol* Chapter 14: Unit14.20
- Eising S, Thiele L, Fröhlich F (2019) A systematic approach to identify recycling endocytic cargo depending on the GARP complex. *Elife* 8: 1–22
- Furuta N, Fujimura-Kamada K, Saito K, Yamamoto T, Tanaka K (2007) Endocytic recycling in yeast is regulated by putative phospholipid translocases and the Ypt31p/32p-Rcy1p pathway. *Mol Biol Cell* 18: 295–312
- Galindo A, Planelles-Herrero VJ, Degliesposti G, Munro S (2021) Cryo-EM structure of metazoan TRAPP3, the multi-subunit complex that activates the GTPase Rab1. *EMBO J* 40: 1–17
- Gallego O, Specht T, Brach T, Kumar A, Gavin AC, Kaksonen M (2013) Detection and characterization of protein interactions in vivo by a simple live-cell imaging method. *PLoS One* 8: 1–6
- Guimaraes RS, Delorme-Axford E, Klionsky DJ, Reggiori F (2015) Assays for the biochemical and ultrastructural measurement of selective and nonselective types of autophagy in the yeast *Saccharomyces cerevisiae*. *Methods* 75: 141–150
- Hanamatsu H, Fujimura-Kamada K, Yamamoto T, Furuta N, Tanaka K (2014) Interaction of the phospholipid flippase Drs2p with the F-box protein Rcy1p plays an important role in early endosome to trans-Golgi network vesicle transport in yeast. *J Biochem* 155: 51–62
- Heider MR, Gu M, Duffy CM, Mirza AM, Marcotte LL, Walls AC, Farrall N, Hakhverdyan Z, Field MC, Rout MP et al (2016) Subunit connectivity, assembly determinants, and architecture of the yeast exocyst complex. *Nat Struct Mol Biol* 23: 59–66
- Hinners I (2003) Changing directions: clathrin-mediated transport between the Golgi and endosomes. *J Cell Sci* 116: 763–771
- Hiraizumi M, Yamashita K, Nishizawa T, Nureki O (2019a) Cryo-EM structures capture the transport cycle of the P4-ATPase flippase. *Science* 365: 1149–1155
- Hiraizumi M, Yamashita K, Nishizawa T, Nureki O (2019b) Cryo-EM structures capture the transport cycle of the P4-ATPase flippase. *Science* 365: 1149–1155. Protein Data Base 6K7N <http://doi.org/10.2210/pdb6K7N/pdb> [DATASET]
- Hua Z, Fatheddin P, Graham TR (2002) An essential subfamily of Drs2p-related P-type ATPases is required for protein trafficking between Golgi complex and endosomal/vacuolar system. *Mol Biol Cell* 13: 3162–3177
- Huh WK, Falvo JV, Gerke LC, Carroll AS, Howson RW, Weissman JS, O'Shea EK (2003) Global analysis of protein localization in budding yeast. *Nature* 425: 686–691
- Janke C, Magiera MM, Rathfelder N, Taxis C, Reber S, Maekawa H, Moreno-Borchart A, Doenges G, Schwob E, Schiebel E et al (2004) A versatile toolbox for PCR-based tagging of yeast genes: new fluorescent proteins, more markers and promoter substitution cassettes. *Yeast* 21: 947–962
- Joiner AM, Phillips BP, Yugandhar K, Sanford EJ, Smolka MB, Yu H, Miller EA, Fromme JC (2021) Structural basis of TRAPP3-mediated Rab1 activation. *EMBO J* 40: 1–19
- Kakuta S, Yamamoto H, Negishi L, Kondo-Kakuta C, Hayashi N, Ohsumi Y (2012) Atg9 vesicles recruit vesicle-tethering proteins Trs85 and Ypt1 to the autophagosome formation site. *J Biol Chem* 287: 44261–44269
- Kao A, Chiu C, Vellucci D, Yang Y, Patel VR, Guan S, Randall A, Baldi P, Rychnovsky SD, Huang L (2011) Development of a novel cross-linking strategy for fast and accurate identification of cross-linked peptides of protein complexes. *Mol Cell Proteomics* 10: M110.002212
- Kukulski W, Schorb M, Welsch S, Picco A, Kaksonen M, Briggs JAG (2011) Correlated fluorescence and 3D electron microscopy with high sensitivity and spatial precision. *J Cell Biol* 192: 111–119
- Kushnirov VV (2000) Rapid and reliable protein extraction from yeast. *Yeast* 16: 857–860
- Laughery MF, Shumaker T, Hunter T, Brown A, Hoopes J, Ostbye T, Wyrick JJ (2015) New vectors for simple and streamlined CRISPR-Cas9 genome editing in *Saccharomyces cerevisiae*. *Yeast* 32: 711–720
- Liu K, Hua Z, Nepute JA, Graham TR (2007) Yeast P4-ATPases Drs2p and Dnf1p are essential cargos of the NPF3D/Slp1p endocytic pathway. *Mol Biol Cell* 18: 487–500
- Liu K, Surendhran K, Nothwehr SF, Graham TR (2008) P4-ATPase requirement for AP-1/Clathrin function in protein transport from the trans-Golgi network and early endosomes. *Mol Biol Cell* 19: 3526–3535
- Lynch-Day MA, Klionsky DJ (2010) The Cvt pathway as a model for selective autophagy. *FEBS Lett* 584: 1359–1366
- Lynch-Day MA, Bhandari D, Menon S, Huang J, Cai H, Bartholomew CR, Brumell JH, Ferro-Novick S, Klionsky DJ (2010) Trs85 directs a Ypt1 GEF, TRAPP3, to the phagophore to promote autophagy. *Proc Natl Acad Sci USA* 107: 7811–7816
- Matoba K, Kotani T, Tsutsumi A, Tsuji T, Mori T, Noshiro D, Sugita Y, Nomura N, Iwata S, Ohsumi Y et al (2020) Atg9 is a lipid scramblase that mediates autophagosomal membrane expansion. *Nat Struct Mol Biol* 27: 1185–1193
- Meiling-Wesse K, Epple UD, Krick R, Barth H, Appelles A, Voss C, Eskelinen EL, Tnumm M (2005) Trs85 (Gsg1), a component of the TRAPP complexes, is required for the organization of the preautophagosomal structure during selective autophagy via the Cvt pathway. *J Biol Chem* 280: 33669–33678
- Morozova N, Liang Y, Tokarev AA, Chen SH, Cox R, Andrejic J, Lipatova Z, Sciorra VA, Emr SD, Segev N (2006) TRAPP2 subunits are required for the specificity switch of a Ypt-Rab GEF. *Nat Cell Biol* 8: 1263–1269
- Müller-Reichert M (2012) *Correlative light and electron microscopy*. Chichester, UK: John Wiley and Sons Ltd

- Nakanishi H, Irie K, Segawa K, Hasegawa K, Fujiyoshi Y, Nagata S, Abe K (2020a) Crystal structure of a human plasma membrane phospholipid flippase. *J Biol Chem* 295: 10180–10194
- Nakanishi H, Nishizawa T, Segawa K, Nureki O, Fujiyoshi Y, Nagata S, Abe K (2020b) Transport cycle of plasma membrane Flippase ATP11C by Cryo-EM. *Cell Rep* 32: 108208
- Natarajan P, Wang J, Hua Z, Graham TR (2004) Drs2p-coupled aminophospholipid translocase activity in yeast Golgi membranes and relationship to in vivo function. *Proc Natl Acad Sci USA* 101: 10614–10619
- Newport TD, Sansom MSP, Stansfeld PJ (2019) The MemProtMD database: a resource for membrane-embedded protein structures and their lipid interactions. *Nucleic Acids Res* 47: D390–D397
- Odorizzi G, Cowles CR, Emr SD (1998) The AP-3 complex: a coat of many colours. *Trends Cell Biol* 8: 282–288
- Perez-Riverol Y, Bai J, Bandla C, García-Seisdedos D, Hewapathirana S, Kamatchinathan S, Kundu DJ, Prakash A, Frericks-Zipper A, Eisenacher M et al (2022) The PRIDE database resources in 2022: a hub for mass spectrometry-based proteomics evidences. *Nucleic Acids Res* 50: D543–D552
- Perkins DN, Pappin DJ, Creasy DM, Cottrell JS (1999) Probability-based protein identification by searching sequence databases using mass spectrometry data. *Electrophoresis* 20: 3551–3567
- Picco A, Irastorza-Azcarate I, Specht T, Böke D, Pazos I, Rivier-Cordey AS, Devos DP, Kaksonen M, Gallego O (2017) The in vivo architecture of the exocyst provides structural basis for exocytosis. *Cell* 168: 400–412.e18
- Protopopov V, Govindan B, Novick P, Gerst JE (1993) Homologs of the synaptobrevin/VAMP family of synaptic vesicle proteins function on the late secretory pathway in *S. cerevisiae*. *Cell* 74: 855–861
- Reggiori F, Wang CW, Stromhaug PE, Shintani T, Klionsky DJ (2003) Vps51 is part of the yeast Vps fifty-three tethering complex essential for retrograde traffic from the early endosome and Cvt vesicle completion. *J Biol Chem* 278: 5009–5020
- Ren Y, Yip CK, Tripathi A, Huie D, Jeffrey PD, Walz T, Hughson FM (2009) A structure-based mechanism for vesicle capture by the multisubunit tethering complex Dsl1. *Cell* 139: 1119–1129
- Saito K, Fujimura-Kamada K, Furuta N, Kato U, Umeda M, Tanaka K (2004) Cdc50p, a protein required for polarized growth, associates with the Drs2p P-type ATPase implicated in phospholipid translocation in *Saccharomyces cerevisiae*. *Mol Biol Cell* 15: 3418–3432
- Sakane H, Yamamoto T, Tanaka K (2006) The functional relationship between the Cdc50p-Drs2p putative aminophospholipid translocase and the Arf GAP Gcs1p in vesicle formation in the retrieval pathway from yeast early endosomes to the TGN. *Cell Struct Funct* 31: 87–108
- Sawa-Makarska J, Baumann V, Coudeville N, von Bülow S, Nogellova V, Abert C, Schuschnig M, Graef M, Hummer G, Martens S (2020) Reconstitution of autophagosome nucleation defines Atg9 vesicles as seeds for membrane formation. *Science* 369: eaaz7714
- Schou KB, Morthorst SK, Christensen ST, Pedersen LB (2014) Identification of conserved, centrosome-targeting ASH domains in TRAPP II complex subunits and TRAPPC8. *Cilia* 3: 6
- Sebastian TT, Baldrige RD, Xu P, Graham TR (2012) Phospholipid flippases: building asymmetric membranes and transport vesicles. *Biochim Biophys Acta* 1821: 1068–1077
- Shirahama-Noda K, Kira S, Yoshimori T, Noda T (2013) TRAPPIII is responsible for vesicular transport from early endosomes to Golgi, facilitating Atg9 cycling in autophagy. *J Cell Sci* 126: 4963–4973
- Siniouoglou S, Pelham HR (2001) An effector of Ypt6p binds the SNARE Tlg1p and mediates selective fusion of vesicles with late Golgi membranes. *EMBO J* 20: 5991–5998
- Stark C, Breitkreutz BJ, Reguly T, Boucher L, Breitkreutz A, Tyers M (2006) BioGRID: a general repository for interaction datasets. *Nucleic Acids Res* 34: D535–S539. BIOGRID-3.2.105 <https://downloads.thebiogrid.org/BioGRID/Release-Archive/BIOGRID-3.2.105/> [DATASET]
- Suvorova ES, Duden R, Lupashin VV (2002) The Sec34/Sec35p complex, a Ypt1p effector required for retrograde intra-Golgi trafficking, interacts with Golgi SNAREs and COPI vesicle coat proteins. *J Cell Biol* 157: 631–643
- Takagi K, Iwamoto K, Kobayashi S, Horiuchi H, Fukuda R, Ohta A (2012) Involvement of Golgi-associated retrograde protein complex in the recycling of the putative Dnf aminophospholipid flippases in yeast. *Communications* 417: 490–494
- Tan D, Cai Y, Wang J, Zhang J, Menon S, Chou H-T, Ferro-Novick S, Reinisch KM, Walz T (2013) The EM structure of the TRAPPIII complex leads to the identification of a requirement for COPII vesicles on the macroautophagy pathway. *Proc Natl Acad Sci USA* 110: 19432–19437
- Teo G, Liu G, Zhang J, Nesvizhskii AI, Gingras A-C, Choi H (2014) SAINTexpress: improvements and additional features in significance analysis of interactome software. *J Proteomics* 100: 37–43
- Thomas LL, Joiner AMN, Fromme JC (2018) The TRAPPIII complex activates the GTPase Ypt1 (Rab1) in the secretory pathway. *J Cell Biol* 217: 283–298
- Timcenko M, Lyons JA, Janulienė D, Ulstrup JJ, Dieudonné T, Montigny C, Ash MR, Karlsen JL, Boesen T, Kühlbrandt W et al (2019a) Structure and autoregulation of a P4-ATPase lipid flippase. *Nature* 571: 366–370
- Timcenko M, Lyons JA, Janulienė D, Ulstrup JJ, Dieudonné T, Montigny C, Ash MR, Karlsen JL, Boesen T, Kühlbrandt W et al (2019b) Structure and autoregulation of a P4-ATPase lipid flippase. *Nature* 571: 366–370. Protein Data Base 6ROH <http://doi.org/10.2210/pdb6ROH/pdb> [DATASET]
- Tinevez JY, Perry N, Schindelin J, Hoopes GM, Reynolds GD, Laplantine E, Bednarek SY, Shorte SL, Eliceiri KW (2017) TrackMate: an open and extensible platform for single-particle tracking. *Methods* 115: 80–90
- Tong Y, Boone C (2005) Synthetic genetic Array analysis in *Saccharomyces cerevisiae*. *Methods Mol Biol* 313: 171–192
- Torreira E, Louro JA, Pazos I, González-Polo N, Gil-Carton D, Duran AG, Tosi S, Gallego O, Calvo O, Fernández-Tornero C (2017) The dynamic assembly of distinct RNA polymerase I complexes modulates rDNA transcription. *eLife* 6: e20832
- Tsai P-C, Hsu J-W, Liu Y-W, Chen K-Y, Lee F-JS (2013) Arl1p regulates spatial membrane organization at the trans-Golgi network through interaction with Arf-GEF Gea2p and flippase Drs2p. *Proc Natl Acad Sci USA* 110: E668–E677
- Wang IH, Chen YJ, Hsu JW, Lee FJS (2017) The Arl3 and Arl1 GTPases cooperate with Cog8 to regulate selective autophagy via Atg9 trafficking. *Traffic* 18: 580–589
- Xu P, Baldrige RD, Chi RJ, Burd CC, Graham TR (2013) Phosphatidylserine flipping enhances membrane curvature and negative charge required for vesicular transport. *J Cell Biol* 202: 875–886
- Yamamoto H, Kakuta S, Watanabe TM, Kitamura A, Sekito T, Kondo-Kakuta C, Ichikawa R, Kinjo M, Ohsumi Y (2012) Atg9 vesicles are an important membrane source during early steps of autophagosome formation. *J Cell Biol* 198: 219–233
- Yip CK, Berscheminski J, Walz T (2010) Molecular architecture of the TRAPPIII complex and implications for vesicle tethering. *Nat Struct Mol Biol* 17: 1298–1304
- Yu I-M, Hughson FM (2010) Tethering factors as organizers of intracellular vesicular traffic. *Annu Rev Cell Dev Biol* 26: 137–156
- Yu S, Liang Y (2012) A trapper keeper for TRAPP, its structures and functions. *Cell Mol Life Sci* 69: 3933–3944

- Zhou X, Sebastian TT, Graham TR (2013) Auto-inhibition of Drs2p, a yeast phospholipid flippase, by its carboxyl-terminal tail. *J Biol Chem* 288: 31807–31815
- Zhou F, Zou S, Chen Y, Lipatova Z, Sun D, Zhu X, Li R, Wu Z, You W, Cong X et al (2017) A Rab5 GTPase module is important for autophagosome clouser. *PLoS Genet* 13: 1–24
- Zimmermann L, Stephens A, Nam SZ, Rau D, Kübler J, Lozajic M, Gabler F, Söding J, Lupas AN, Alva V (2018) A completely reimplemented MPI bioinformatics toolkit with a new HHpred server at its Core. *J Mol Biol* 430: 2237–2243
- Zou S, Chen Y, Liu Y, Segev N, Yu S, Liu Y, Min G, Ye M, Zeng Y, Zhu X et al (2013) Trs130 participates in autophagy through GTPases Ypt31/32 in *Saccharomyces cerevisiae*. *Traffic* 14: 233–246

- Zuo X, Guo W, Lipschutz JH (2009) The exocyst protein Sec10 is necessary for primary ciliogenesis and cystogenesis in vitro. *Mol Biol Cell* 20: 2522–2529



License: This is an open access article under the terms of the [Creative Commons Attribution-NonCommercial-NoDerivs](https://creativecommons.org/licenses/by-nc-nd/4.0/) License, which permits use and distribution in any medium, provided the original work is properly cited, the use is non-commercial and no modifications or adaptations are made.

Expanded View Figures

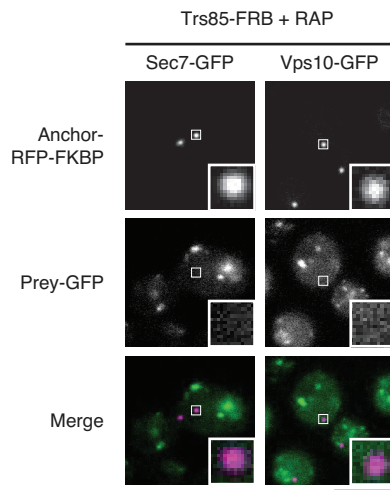


Figure EV1. PICT assay for the interactions between TRAPPIII and proteins located at the TGN.

Representative images of the PICT assay obtained from the screening shown in Fig 1 (Dataset EV1) for the interaction of Trs85-FRB (TRAPPIII) and Sec7-GFP or Vps10-GFP after adding rapamycin (RAP). RFP-tagged anchor and GFP-tagged prey are shown in the upper and middle row, respectively. Bottom row shows the merged images. White zoom in boxes, 0.9 μm . Scale bar, 5 μm .

Source data are available online for this figure.

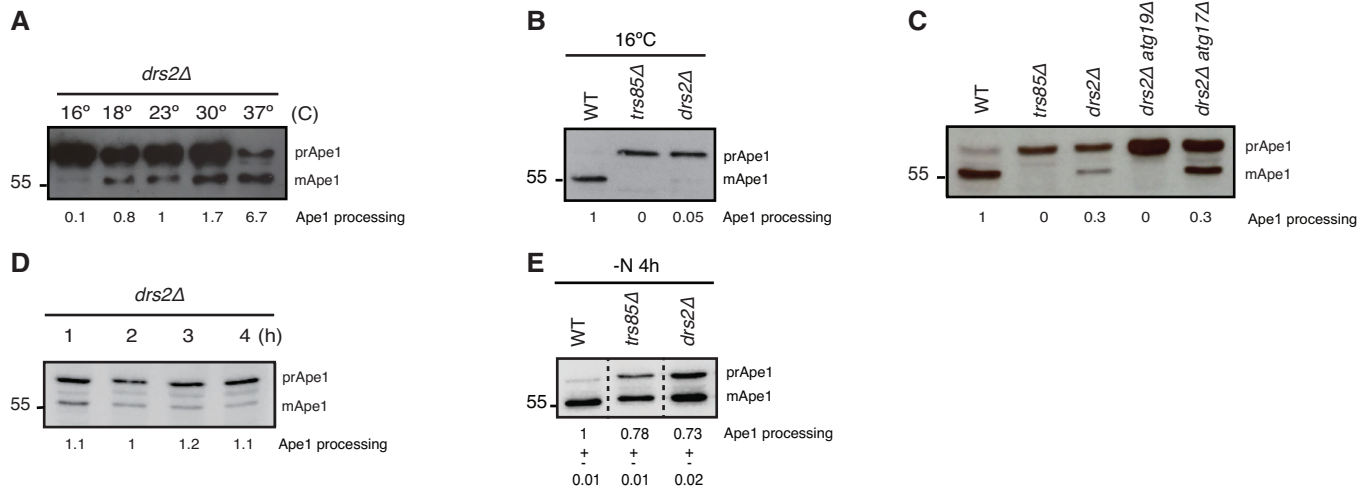


Figure EV2. Drs2 is essential for the Cvt pathway as the temperature decreases.

Ape1 processing was analyzed by Western blot in the indicated strains.

A *drs2Δ* cells were grown at 30°C and then cultured for 2 h at the indicated temperatures.

B Wild-type, *trs85Δ* and *drs2Δ* cells were grown at 30°C and then cultured for 2 h at 16°C.

C Analysis of Ape1 processing in *drs2Δ* cells where either the Cvt pathway (*atg19Δ*) or nonselective autophagy (*atg17Δ*) were blocked.

D *drs2Δ* cells were grown at 30°C and then cultured for 1, 2 or 4 h at 23°C.

E Wild-type, *trs85Δ* and *drs2Δ* cells were grown at 30°C and then cultured for 4 h at 23°C without a nitrogen source to analyze the effect of nonselective autophagy.

Data information: (A, D) Below, Ape1 processing was normalized to the processing achieved after 2 h at 23°C. (B, C, E) Below, Ape1 processing was normalized to the processing achieved in wild-type cells.

Source data are available online for this figure.

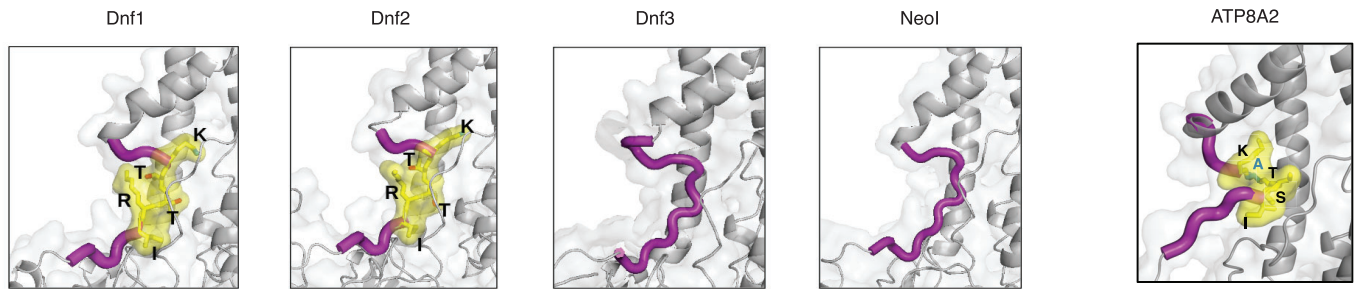


Figure EV3. Modeling of the N-terminal cavity of P4-ATPases.

Structural representation of the 15 aa cavity (purple) in the N-terminal tail of Dnf1 (15.5 × 9.4 Å), Dnf2 (11.6 × 9.5 Å), Dnf3 (13.5 × 15.5 Å) and Neo1 (18.1 × 13.8 Å). Drs2 was used as a template PDB ID: 6ROH:A (Timcenko et al, 2019a; Data ref: Timcenko et al, 2019b). The I(S/R)TTK motif present in Dnf1 and Dnf2 is highlighted in yellow. Structural representation of the 15 aa cavity (purple) in the N-terminal tail of the human ATP8A2 (17.7 × 20.5 Å). ATP8A1 was used as a template (PDB ID: 6K7N; Hiraizumi et al, 2019a; Data ref: Hiraizumi et al, 2019b). The ISTAK motif is highlighted in yellow. The only mismatch with the I(S/R)TTK motif is labeled in blue.

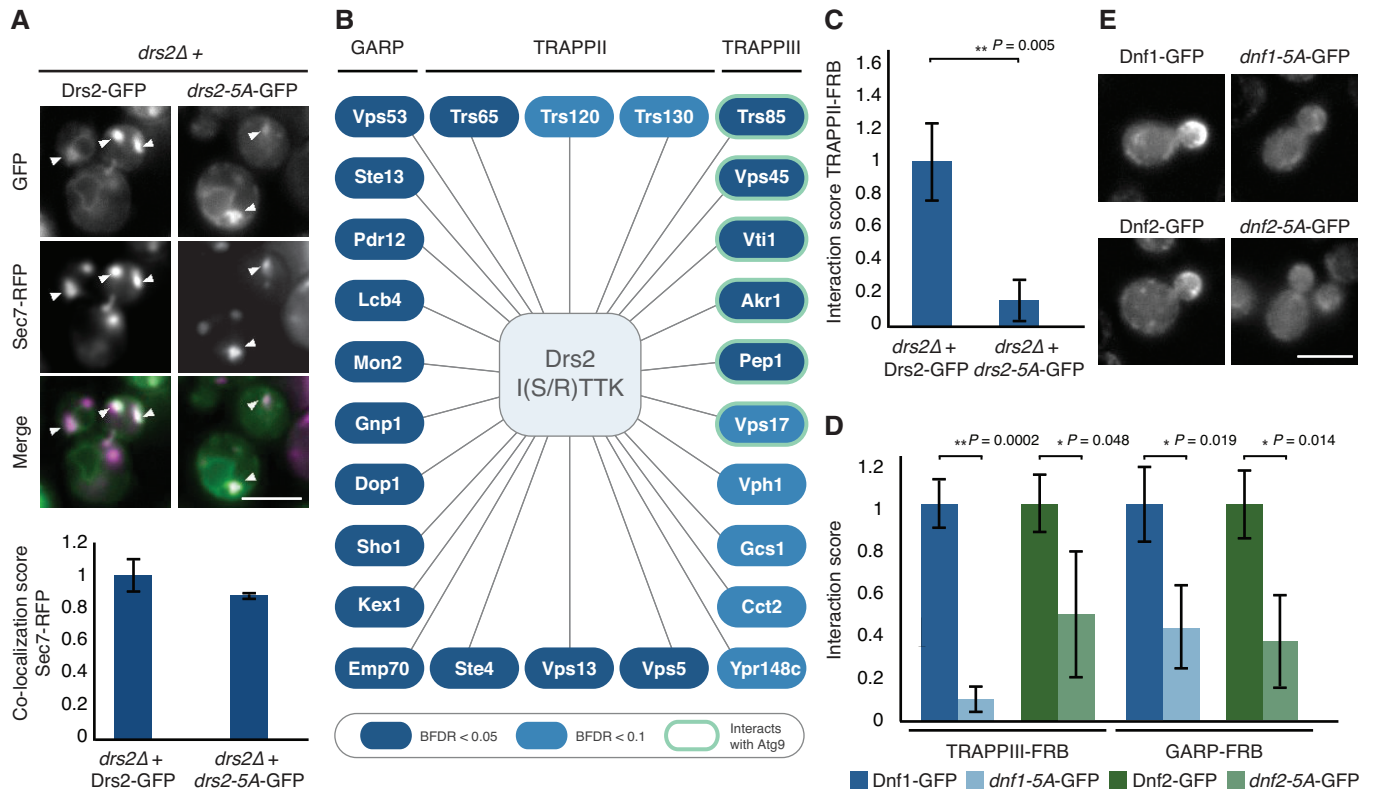


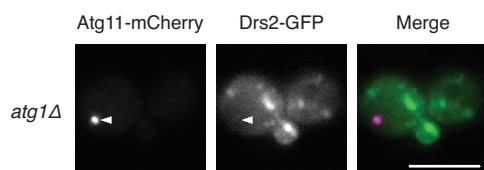
Figure EV4.

Figure EV4. The role of the I(S/R)TTK motif.

- A Representative images (top) and quantification (bottom) of the co-localization between Sec7-RFP and Drs2-GFP or *drs2-5A*-GFP in *drs2Δ* cells. White arrowheads point to Sec7-RFP clusters co-localizing with Drs2-GFP or *drs2-5A*-GFP. Scale bar, 5 μ m. Values were normalized to the measurements in cells expressing wild-type Drs2.
- B Graphic representation of the 26 proteins whose interaction with Drs2 is diminished by the mutation of the I(S/R)TTK motif in XL-MS experiments. Binding to Atg9 as reported in SGD (Data ref: Saccharomyces Genome Database, 2021). BFDR, Bayesian False Discovery Rate.
- C Interaction between Trs130-FRB and Drs2-GFP or *drs2-5A*-GFP analyzed by PICT. The Interaction score was normalized to the measurement of Drs2-GFP.
- D Interaction of either Trs85-FRB or Vps53-FRB with Dnf1-GFP, *dnf1-5A*-GFP, Dnf2-GFP or *dnf2-5A*-GFP analyzed by PICT. The Interaction score was normalized to the measurement of Dnf1-GFP or Dnf2-GFP.
- E Representative images of Dnf1-GFP, *dnf1-5A*-GFP, Dnf2-GFP or *dnf2-5A*-GFP.

Data information: (A, C, E) Error bars: mean \pm SD, $n = 3$ biological replicates. Asterisk indicates significant difference as determined by a two-tailed Student's t -test (* $P < 0.05$; ** $P < 0.01$).

Source data are available online for this figure.

**Figure EV5. GFP-tagged Drs2 do not localize with the PAS marker Atg11.**

Representative images of the co-localization between Atg11 tagged to mCherry and Drs2-GFP in cells lacking the kinase Atg1, required for the Cvt vesicle formation ($n = 3$). Arrowhead points to an Atg11-mCherry spot. Scale bar, 5 μ m. Source data are available online for this figure.